



Article

Multiple-Win Effects and Beneficial Implications from Analyzing Long-Term Variations of Carbon Exchange in a Subtropical Coniferous Plantation in China

Jianhui Bai ^{1,*} , Fengting Yang ², Huimin Wang ², Lu Yao ¹  and Mingjie Xu ³

¹ LAGEO, Institute of Atmospheric Physics, Chinese Academy of Sciences (IAP, CAS), Beijing 100029, China; yaolu@mail.iap.ac.cn

² Key Laboratory of Ecosystem Network Observation and Modeling, Institute of Geographic Sciences and Natural Resources Research, CAS, Beijing 100101, China; yangft@igsnr.ac.cn (F.Y.); wanghm@igsnr.ac.cn (H.W.)

³ College of Agronomy, Shenyang Agricultural University, Shenyang 110866, China; xumj@syau.edu.cn

* Correspondence: bjh@mail.iap.ac.cn

Abstract: To improve our understanding of the carbon balance, it is significant to study long-term variations of all components of carbon exchange and their driving factors. Gross primary production (GPP), respiration (Re), and net ecosystem productivity (NEP) from the hourly to the annual sums in a subtropical coniferous forest in China during 2003–2017 were calculated using empirical models developed previously in terms of PAR (photosynthetically active radiation), and meteorological parameters, GPP, Re, and NEP were calculated. The calculated GPP, Re, and NEP were in reasonable agreement with the observations, and their seasonal and interannual variations were well reproduced. The model-estimated annual sums of GPP and Re over 2003–2017 were larger than the observations of 11.38% and 5.52%, respectively, and the model-simulated NEP was lower by 34.99%. The GPP, Re, and NEP showed clear interannual variations, and both the calculated and the observed annual sums of GPPs increased on average by 1.04% and 0.93%, respectively, while the Re values increased by 4.57% and 1.06% between 2003 and 2017. The calculated and the observed annual sums of NEPs/NEEs (net ecosystem exchange) decreased/increased by 1.04%/0.93%, respectively, which exhibited an increase of the carbon sink at the experimental site. During the period 2003–2017, the annual averages of PAR and the air temperature decreased by 0.28% and 0.02%, respectively, while the annual average water vapor pressure increased by 0.87%. The increase in water vapor contributed to the increases of GPP, Re, and NEE in 2003–2017. Good linear and non-linear relationships were found between the monthly calculated GPP and the satellite solar-induced fluorescence (SIF) and then applied to compute GPP with relative biases of annual sums of GPP of 5.20% and 4.88%, respectively. Large amounts of CO₂ were produced in a clean atmosphere, indicating a clean atmospheric environment will enhance CO₂ storage in plants, i.e., clean atmosphere is beneficial to human health and carbon sink, as well as slowing down climate warming.

Keywords: CO₂ balance; gross primary production; respiration; net ecosystem productivity; empirical model; solar-induced fluorescence



Citation: Bai, J.; Yang, F.; Wang, H.; Yao, L.; Xu, M. Multiple-Win Effects and Beneficial Implications from Analyzing Long-Term Variations of Carbon Exchange in a Subtropical Coniferous Plantation in China.

Atmosphere **2024**, *15*, 1218. <https://doi.org/10.3390/atmos15101218>

Academic Editors: Jimmy O. Adegoke and Jane Liu

Received: 4 September 2024

Revised: 6 October 2024

Accepted: 9 October 2024

Published: 12 October 2024



Copyright: © 2024 by the authors. Licensee MDPI, Basel, Switzerland. This article is an open access article distributed under the terms and conditions of the Creative Commons Attribution (CC BY) license (<https://creativecommons.org/licenses/by/4.0/>).

1. Introduction

Global warming (especially in the most sensitive regions, including Three Polar) and its causes are a great concern for governments and scientists [1–6]. Global CO₂ concentrations are rising since the Industrial Revolution in the 19th century. CO₂ accounts for 70% of greenhouse gas (GHG) emissions [7], and its emission should be critically controlled in the processes to achieve regional and global carbon neutrality [8,9]. It is also vital to thoroughly investigate the regional and global ecosystem carbon balance and their long-term variations, as the terrestrial biosphere can sequester 20%–30% of global anthropogenic CO₂ emissions [10].

As a reliable technique, the eddy covariance (EC) is extensively used to measure and validate CO₂ exchange during different time scales (half-hour to several tens of years) at sites with different types of terrain in the world, such as ChinaFLUX, AsiaFlux, AmeriFLUX, and CARBOEUROPE [11–19]. Flux data are further commonly used in carbon cycle model developments and evaluations, investigating the processes, mechanisms, and potential effects of CO₂ on climate change. Though much progress has been made, there are still challenges in EC measurements and model simulations, especially how to reduce their large uncertainties [20] and how to improve data quality [19,21,22]. The problem of surface energy imbalance/nonclosure still needs to be better resolved [23–25]. Thus, it is important to comprehensively study long-term variations and reasons for carbon balance and its driving factors.

Based on measurements of net carbon exchange, many types of models are developed and applied to (1) calculate net ecosystem exchange (NEE), net ecosystem productivity (NEP), respiration (Re), and gross primary production (GPP) [26–35]; (2) analyze their variations [35–41]; and (3) investigate their responses to the driving factors (light, temperature, water, drought, land cover change, etc.) [26–29,38–41]. These models include empirical models, sophisticated models [32,42–44], and atmospheric inversions [45,46]. The process-based dynamic global vegetation models (DGVMs) are commonly used to compute the land carbon sink in reasonable line with the global carbon budget. Remote sensing and geographic information system (GIS) data-based methods provide useful tools to study carbon balance. Machine-learning algorithms (e.g., extreme gradient boosting (XGBoost) and artificial neural networks (ANN)) are also applied as promising methods [47–49]. Although much progress has been made, there are still large differences between different models [44] and large uncertainties in CO₂ flux observations and model predictions [11,50–55]. Additionally, many hypotheses are still used in complex models [56]. Respiration is an important part of carbon cycling [57] and is necessary to be well studied, e.g., the partitioning between the components of the CO₂ atmospheric budget [58]. NEP (or NEE) as a significant indicator of ecosystem carbon source and sink should be evaluated as well.

The greening pattern during 2000–2017 worldwide is markedly evident in China [59]. To fulfill carbon peak and carbon neutrality, more and more plants and grasses will be cultivated in China. China hosts several typical ecosystems, and great progress has been achieved by Chinese scientists on China's land carbon exchange. For example, the number of sites in the ChinaFLUX network between 2002 and 2022 increased to 81, including 25 forest stations, 19 grassland stations, and 18 agriculture stations. Numerous flux tower measurement and model studies, along with fruitful results, have been conducted [27,30,31,33,35–37,39]. Since 1982, 1.65 ± 0.76 PgC has been stored in forest [60]. Further studies are required to investigate ecosystems' carbon budgets, especially the long-term variations of GPP, Re, and NEP [27,39,61] and the reasons for these variations [26,60–63]. It will benefit us to make effective policies to achieve the Dual Carbon Goals, along with air pollution reduction. Satellite remote sensing provides useful information to study carbon balance and its related issues over large space. Satellite solar-induced fluorescence (SIF) as a by-product of photosynthesis and an effective proxy for plant photosynthesis has been applied to calculate GPP for ecosystems [64,65] and to monitor plant stress and growth states [66,67]. Through correlation analysis with satellite and in situ GPP, the SIF product shows good performance in estimating GPP [68].

This study made further progress based on our previous ones [40,41] and applied our developed empirical models to investigate long-term variation features of carbon balance in the Qianyanzhou forest region. More introductions about EC measurements and their uncertainties, model simulations, and their uncertainties of GPP, Re, and NEP/NEE are reported in studies [40,41].

As an important carbon sink, a subtropical coniferous forest in China was chosen for this study. Our aims were to study the long-term variations of GPP, Re, and NEP over 15 years, as well as their variation patterns and mechanisms, and then propose

suggestions for achieving win–win effects in dual carbon goals, reducing air pollutants, and slowing down climate warming. Therefore, we (1) estimated GPP, Re, and NEP values in 2003–2017 with the applications of our previously developed empirical models of GPP, Re, and NEP (EMGPP, EMRe, EMNEP) and the use of the observed solar radiation and meteorological variables, (2) further evaluated the performances of EMGPP, EMRe, and EMNEP, (3) studied long-term variations of GPP, Re, and NEP during 2003–2017 and analyzed the reasons between their simulations and observations, as well as providing some beneficial recommendations, (4) investigated the reasons for their variations due to their driving factors, (5) investigated (a) GPP under different atmospheric conditions and which condition is the best to improve carbon storage in the forests and (b) is there any way to store more carbon in the plants and improve air quality? Then, (6) quantified the relationships between GPP and SIF and applied them to estimate GPP.

2. Instrumentation and Methods

2.1. Site Description

CO₂ fluxes, solar radiation, and meteorological parameters were measured at a 45 m tower in the Qianyanzhou subtropical coniferous forest, Taihe County, Jiangxi Province (26°44′48″ N, 115°04′13″ E) in China (Figure 1) since 2003 [69]. Solar radiation, meteorological variables, and BVOC (biogenic volatile organic compounds) emission fluxes were also observed at this tower from 22 May, 2013–4 January, 2016 [70]. Around the tower, the dominant trees and shrubs, forest coverage, canopy height, and mean slope are introduced in [70]. Annual total precipitation is 1485.1 mm and annual mean air temperature is 17.9 °C [71]. The annual totals of global solar radiation and PAR are 4579 MJ m⁻² and 7998 mol m⁻² in 2013, respectively [70].

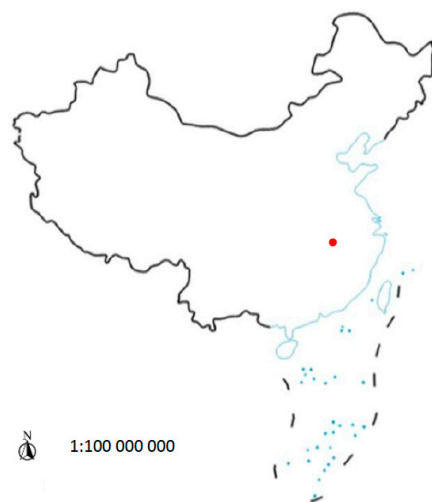


Figure 1. A sketch map about the site of Qianyanzhou subtropical coniferous forest (red point), located in Taihe County, Jiangxi Province, China.

2.2. Instruments and Measurements

The EC system is composed of a 3-D sonic anemometer (Model CSAT3, Campbell Scientific Inc., Logan, UT, USA), an open-path CO₂/H₂O analyzer (Model LI-7500, Li-COR Inc., Lincoln, NE, USA), and a CR5000 datalogger (Campbell Scientific Inc., Logan, UT, USA). The EC system is installed at 23.6 and 39.6 m above ground to measure CO₂ flux in Qianyanzhou subtropical coniferous forest [69,72], and the hourly observational data (NEE/NEP, Re, and GPP) at 23.6 m from 1 January 2003, to 31 December 2017, were used in this study. Radiation (upward and downward short wave solar radiation, and upward and downward longwave radiation) and PAR were measured using radiometers (a four-component net radiometer, model CNR1, Kipp and Zone, Delft, ZuidHolland, the Netherlands; LI-190SB Quantum Sensor, LI-COR, Inc., Lincoln, NE, USA) and recorded

by a data-collection system (41.6 m for shortwave and longwave solar radiation, and 23.6 m for PAR). Solar radiation (global radiation Q , direct radiation D , scattered radiation $S = Q - D \times \cos(Z)$, Z is the solar zenith angle, and PAR) and meteorological variables were also measured by another set of solar radiation systems (Bai's group) from 21 May 2013–31 December 2016, at the Qianyanzhou station [70]. Meteorological variables (air temperature (T , °C), relative humidity (RH, %), and water vapor pressure (E , hPa)) from 2003–2017 were obtained using a sensor (HMP45C, Vaisala, Helsinki, Finland) [72,73]. Figure 2 displays CO₂ flux, solar radiation, and meteorological measurement instruments operated by the Qianyanzhou experimental station and Bai's group, respectively.



Figure 2. The eddy covariance (EC, **up left**) and solar radiation measurement (**up right**) systems in Qianyanzhou subtropical coniferous forest operated by the Qianyanzhou experimental station. Another set of solar radiation (global radiation, direct radiation, and PAR) measurement systems (**bottom left**) located at a top of the building, and a HOBO weather station (**bottom right**) located at a meteorological observation station operated by Bai's group.

2.3. Processing and Usage of Flux Data

ChinaFLUX has used several mature methods to study the performance of the observational system and data quality [40,72,74]. The methods of raw data processing, data gap filling of CO₂ flux in the daytime and nighttime, and the threshold have been fully reported [40,72,75–80] and were employed in this study.

In this study, a multi-source-driven SIF product (named GOSIF) was used to evaluate the relationship between SIF and GPP [81], which is based on Orbiting Carbon Observatory-2 (OCO-2) SIF data, Moderate Resolution Imaging Spectroradiometer (MODIS) vegetation index data, and Modern-Era Retrospective analysis for Research and Application (MERRA-2) meteorological data. The SIF product provides a spatial resolution of 0.05° and a temporal resolution of 8 days on a global scale (see GOSIF website at <https://globalecology.unh.edu/data/GOSIF.html>, accessed on 1 October, 2024). The long time series of the SIF product with a temporal extent from 2000 to 2022 makes it a powerful dataset for ecosystem change

research. Here, we have selected the SIF product at 8-day temporal for the period from 2003 to 2017 within a 1° radius of the Qianyanzhou station to analyze the relationships between SIF and GPP under different atmospheric conditions.

2.4. Applications of Empirical Models of GPP, Re, and NEP

On the basis of the PAR balance principle, the empirical models (EMGPP, Equation (1); EMRe, Equation (2); EMNEP, combined Equations (1) and (2), $NEP = GPP - Re$) in Qianyanzhou subtropical coniferous forest have been developed using the hourly observational data (fluxes measured by the Qianyanzhou station, PAR, S/Q, and meteorological parameters measured by Bai's group) from 22 May 2013–31 December 2014. These empirical models were then used to calculate GPP, Re, and NEP from 1 January 2013–31 December 2016, also using hourly solar radiation and meteorological parameters measured by Bai's group. Their simulations were compared and evaluated in different ways (from hourly to daily, monthly, and annual values in different years, 2013–2016) and showed reasonable performances (the statistical metrics, including coefficient of determination (R^2), average and maximum of the absolute relative bias, normalized mean square error (NMSE), standard deviations of calculated and observed fluxes, mean absolute deviations (MAD), and root mean square errors (RMSE)) of GPP, Re, and NEP (including the hourly, daily, monthly, and annual values), and reproducibility of their seasonal and annual variations from 2013–2016 [40,41]. Considering the limitation of direct or diffuse solar radiation at stations in China, 2-factor empirical models of GPP, Re, and NEP (i.e., without scattering term) were also developed for their practical applications. Generally, the simulations of GPP, Re, and NEP were in reasonable agreement with the measurements (e.g., 20–50% for CO_2 flux measurements) and popular used models (e.g., standard deviations of calculated and observed fluxes, RMSE). The RMSE simulated using the Yale Interactive Terrestrial Biosphere (YIB) model was $3.21 \text{ gC m}^{-2} \text{ day}^{-1}$ (57 evergreen coniferous forests), which is in good line with that of 3.55 and $3.44 \text{ gC m}^{-2} \text{ day}^{-1}$ from 2013–2016, which was calculated using 3-factor and 2-factor EMGPP [40]. Annual GPP, RE, and NEP estimates overestimated the observations from 2013–2016 by 31% and 29% for GPP, 30% for Re, and 22.0% and 27.0% for NEP, respectively, using the 3-factor and 2-factor models [40,41]. In more detail, the empirical models (EMGPP, EMRe, and EMNEP) considered the two atmospheric conditions (described by a scattering factor, S/Q), $S/Q < 0.5$ and $S/Q \geq 0.5$, representing low or high gas, liquid, and particle (GLP) loads in the atmosphere, corresponding to a clean atmosphere (low amounts of clouds, aerosols, etc., along with strong solar radiation and high air temperature) or misty atmosphere (a large number of clouds, aerosols, etc., as well as low solar radiation and air temperature), respectively, and combined them together for the simulations of GPP, RE, and NEP under realistic atmospheric conditions ($S/Q = 0-1$).

$$e^{-0.1aGPPtm} \times \cos(Z) = A_1PAR + A_2e^{-kWm} \times \cos(Z) + A_3e^{-S/Q} + A_0 \quad (1)$$

$$e^{-0.1bRetm} \times \cos(Z) = B_1PAR + B_2e^{-kWm} \times \cos(Z) + B_3e^{-S/Q} + B_0 \quad (2)$$

where in the GPP term ($e^{-0.1aGPPtm}$), the attenuation coefficient for CO_2 in the atmosphere is $1 \text{ mg CO}_2^{-1} \text{ m}^2 \text{ s}^{-1}$, m is the optical air mass, GPP ($\text{mg CO}_2 \text{ m}^{-2} \text{ s}^{-1}$) is the hourly GPP in the sampling period (t, h), and 0.1 is a normalizing coefficient for GPP. In the photochemical term (e^{-kWm}), $W = 0.021E \times 60$, E is the average water vapor pressure (hPa) at ground during the sampling period and k is the mean absorption coefficient of water vapor ($0.70-2.845 \mu\text{m}$). In the scattering term ($e^{-S/Q}$), S/Q describes the relative amounts of atmospheric GLPs. $b = 1 \text{ mg CO}_2^{-1} \text{ m}^2 \text{ s}^{-1}$. Re is the hourly respiration in the sampling period. Coefficients of A_i and B_i are determined using hourly observational datasets (solar radiation, water vapor pressure, GPP, and Re). More detailed results about the empirical model (EMGPP, EMRe, and EMNEP) developments and evaluations are reported in references [40,41].

Based on previously reasonable simulations of GPP, Re, and NEP from 2013–2016 [40,41], these empirical models (EMGPP, EMRe, and EMNEP) were further applied to investigate

GPP, Re, and NEP and their long-term variations from 1 January 2003–31 December 2017 in this forest using the hourly observational data (CO₂ fluxes, solar radiation, and meteorological variables) measured by the Qianyanzhou station. Figure 3 shows a graphical diagram of the study.

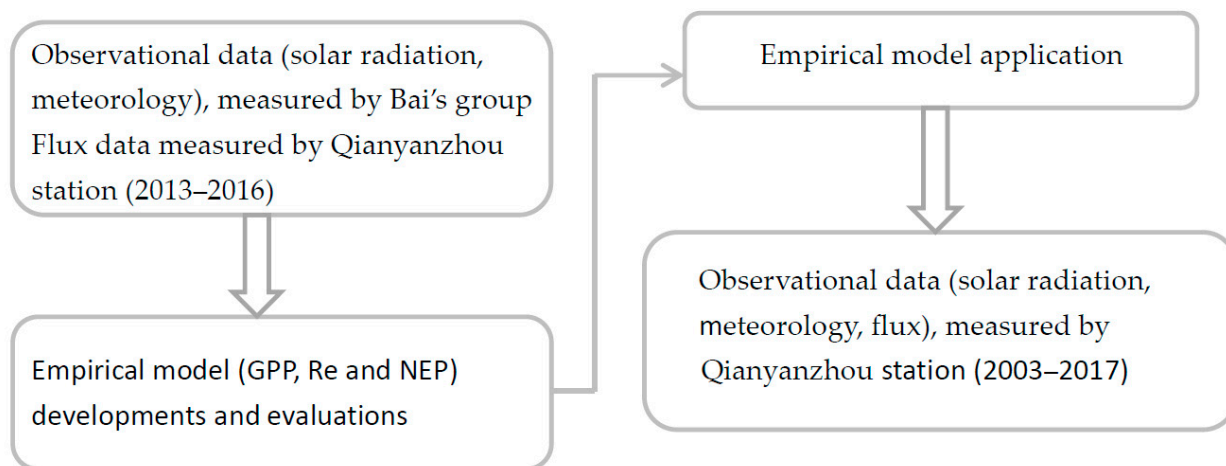


Figure 3. A graphical diagram of the study.

Firstly, the hourly GPP and Re values from 2003–2017 under all sky conditions were computed using the 2-factor EMGPP and EMRe, respectively, considering the direct solar radiation was not measured by the Qianyanzhou station. Secondly, the hourly NEPs under all sky conditions were calculated as the difference between GPP and Re (NEP = GPP – Re).

Under all sky conditions, two types of atmospheric conditions ($S/Q < 0.5$ and $S/Q \geq 0.5$) were also considered. The EMGPP or EMRe used different coefficients to describe different roles of PAR and photochemical terms to GPP or Re in two S/Q situations, respectively [40,41].

Due to the lack of S/Q from 2003–2017, AF factor (Equation (3)) was used as an indicator of S/Q and to identify atmospheric conditions (i.e., high or low GLPs).

$$AF_i = 1 - PAR_i \times m / PAR_{Mmax} \quad (3)$$

where AF_i and PAR_i were hourly averages of AF and the observed PAR during one h, respectively. PAR_{Mmax} is the maximum of the observed PAR in a month.

When using the empirical models of GPP and Re, $AF_i < 0.5$ and ≥ 0.5 were applied to represent the conditions of $S/Q < 0.5$ and $S/Q \geq 0.5$, respectively, and combined considering PAR level (high or low). The range of AF_i was from 0 to 1, corresponding to that of S/Q from 0 to 1.

3. Results

3.1. Model Simulations of GPP, Re, and NEP under All Sky Conditions from 2003–2017

Under all sky conditions, the hourly GPP, Re, and NEP values were estimated using the 2-factor empirical models of GPP, Re, and NEP, respectively, together with the measured PAR and water vapor pressure as inputs. The coefficients of EMGPP or EMRe for two atmospheric conditions ($S/Q < 0.5$ or $S/Q \geq 0.5$), and their combination were suitable to the realistic S/Q situations (identified using AF as $AF < 0.5$ or $AF \geq 0.5$ in this study), which were used to investigate variations of GPP, Re, and NEP for relatively clean, polluted, and realistic atmospheric conditions ($S/Q = 0-1$), respectively. These corresponding simulations of GPP, Re, and NEP were expressed as GPP_{cal1} , GPP_{cal2} , GPP_{cal3} , Re_{cal1} , Re_{cal2} , Re_{cal3} , NEP_{cal1} , NEP_{cal2} , and NEP_{cal3} , respectively.

3.1.1. Hourly Simulations of GPP, Re, and NEP

The hourly GPP, Re, and NEP values from 1 January, 2003, to 31 December, 2017, were calculated using EMGPP, EMRe, and their combinations (i.e., $NEP = GPP - Re$) for

atmospheric conditions at $AF < 0.5$ and $AF \geq 0.5$, as well as realistic atmospheric conditions, respectively. Tables 1 and 2 show their hourly results and statistical metrics, including averages of calculated and observed GPP, Re, and NEP, the ratios of the calculated to the observed value (cal/obs), standard deviations of calculated and observed fluxes (σ_{cal} and σ_{obs}), mean absolute deviations (MAD, in $\text{mgCO}_2 \text{ m}^{-2} \text{ s}^{-1}$ and percentage of the mean measured value, %), and root mean-square errors (RMSE, in $\text{mgCO}_2 \text{ m}^{-2} \text{ s}^{-1}$ and the percentage of mean measured value).

Table 1. Hourly mean estimates of GPP, respiration (Re), and net ecosystem productivity (NEP) (shown in lines 2, 3, and 4) under relatively clean, polluted, and realistic atmospheric conditions (cal1, cal2, cal3), respectively, and their observed values (obs) in a subtropical coniferous plantation from 2003–2017, statistical metrics, i.e., the averages of the calculated and observed GPP, the corresponding ratios of the calculated to observed GPP (cal/obs, R_1 , R_2 , R_3), normalized mean-square error (NMSE), standard deviations of calculated, and observed GPP (σ_{cal} and σ_{obs}), together with mean bias errors (MAD, $\text{mgCO}_2 \text{ m}^{-2} \text{ s}^{-1}$, and %) and root mean-square errors (RMSE, $\text{mgCO}_2 \text{ m}^{-2} \text{ s}^{-1}$, and %).

RMSE		MAD		σ_{obs}	σ_{cal}	NMSE	R_3	R_2	R_1	obs	cal3	cal2	cal1	Model
(%)	($\text{mgCO}_2 \text{ m}^{-2} \text{ s}^{-1}$)	(%)	($\text{mgCO}_2 \text{ m}^{-2} \text{ s}^{-1}$)											
69.51	0.301	52.75	0.228	0.299	0.333	0.434	1.114	1.035	1.931	0.433	0.482	0.447	0.835	EMGPP
174.98	0.367	141.04	0.215	0.073	0.320	2.888	1.060	0.592	3.611	0.153	0.162	0.090	0.551	EMRe
41.58	0.247	35.85	0.213	0.259	0.155	0.265	0.651	0.598	0.472	0.998	0.761	0.727	0.761	EMNEP

Table 2. Same as Table 1, but for daily GPP, Re, and NEP simulations.

RMSE		MAD		σ_{obs}	σ_{cal}	NMSE	R_3	R_2	R_1	obs	cal3	cal2	cal1	Model
(%)	($\text{mgCO}_2 \text{ m}^{-2} \text{ s}^{-1}$)	(%)	($\text{mgCO}_2 \text{ m}^{-2} \text{ s}^{-1}$)											
55.81	2.643	42.82	2.028	2.372	3.338	0.280	1.114	1.035	1.931	4.736	5.276	4.901	9.144	EMGPP
151.01	2.533	126.42	2.121	0.801	3.192	2.159	1.056	0.592	3.611	1.678	1.771	0.993	6.058	EMRe
39.06	2.547	34.99	2.282	1.411	0.608	0.235	0.650	0.599	0.473	6.522	4.240	3.906	3.084	EMNEP

3.1.2. Daily Sum Simulations of GPP, Re, and NEP

The daily sums of GPP, Re, and NEP from 2013–2017 were obtained from their sums of hourly values. The results are shown in Table 2. The RMSE and MAD for daily sums and hourly average of Re were much larger than that of GPP and NEP, and it was mainly caused by the lower Re values compared to that of GPP and NEP. Generally, the daily sums of GPP, Re, and NEP agreed with the observations under realistic atmospheric conditions. For example, the empirical models overestimated the observed (mean) GPP and Re by 11.4% and 5.6%, respectively, and they underestimated the (mean) observed NEP by 35.0%. In contrast, the empirical models overestimated the (mean) observed GPP and Re by a factor of 1.93 and 3.61 for relatively clean atmospheric conditions (low GLP loads) and 1.04 and 0.59 for more polluted atmospheric conditions (high GLP loads), respectively. This indicates that GPP would increase evidently under a relatively clean atmosphere and decrease under a more polluted atmosphere. In other words, more CO_2 (e.g., GPP) would be produced by increased PAR utilization through vegetation photosynthesis and microorganism activity (respiration, e.g., bacterial decomposition of a litter) and then stored in the ecosystem under a clean atmosphere. The empirical models exhibited similar performances for polluted atmospheric conditions as for realistic atmospheric conditions, and it was attributed to the closer GLP loads, e.g., the atmosphere was in high GLP levels in Qianyanzhou coniferous plantation from 2003–2017.

It is found that RMSE values were 2.60 gC m^{-2} and 55.81% for the simulations of the mean daily sums of GPP from 2003–2017, which reasonably agreed with the simulations from 2013–2016, 3.55 gC m^{-2} and 87.60% using the 3-factor EMGPP and solar radiation and meteorological inputs measured by another measurement system (Bai’s group), and 3.43 gC m^{-2} and 83.23% using the 2-factor EMGPP, respectively [40]. Under all sky conditions, the simulated Re values were higher than the observations from 2003–2017, similar to those from 2013–2016. However, the NEP simulations were underestimated from 2003–2017, which were different from that (overestimation) from 2013–2016, i.e., the calculated Re values overestimated the observations by $\sim 30\%$ for the mean hourly and annual sums in 4 years [41].

3.1.3. Monthly Sum Simulations of GPP, Re, and NEP

Similarly, the monthly sum simulations of GPP, Re, and NEP were computed and displayed in Figures 4–6. The empirical models of GPP, Re, and NEP can capture their seasonal variations under three atmospheric situations: higher in summer and lower in winter. It was found that (1) much higher carbon was predicated (about two times the observed GPP) under relatively clean atmospheric conditions (low S/Q , monthly mean ratio $\text{GPP}_{\text{cal1}}/\text{GPP}_{\text{obs}}$ from 2003–2017 = 1.93), e.g., a clean atmosphere is beneficial to carbon dioxide storage in the plants; (2) this ratio was 1.04 and 1.11 for polluted (high S/Q) and realistic atmospheric conditions, i.e., less GPP was fixed in the ecosystem under polluted atmosphere or high GLP load conditions. Therefore, a cleaner atmosphere and reducing high GLP loads in the atmosphere are synergistically effective and beneficial methods to enhance carbon storage in the ecosystem. A similar result is also reported by Yang et al. [82]. (3) the simulated GPP values (GPP_{cal3}) under realistic atmospheric conditions were in reasonable line with the observations, and most of the GPP_{cal3} were within two times standard deviations of the observed GPPs. (4) similar simulations as GPP_{cal3} were also obtained for GPP_{cal2} , revealing that the realistic atmospheric conditions were close to that under high GLPs conditions (i.e., $S/Q \geq 0.5$), i.e., the atmospheric and environmental conditions in the Danzhou Region were under high GLP loads.

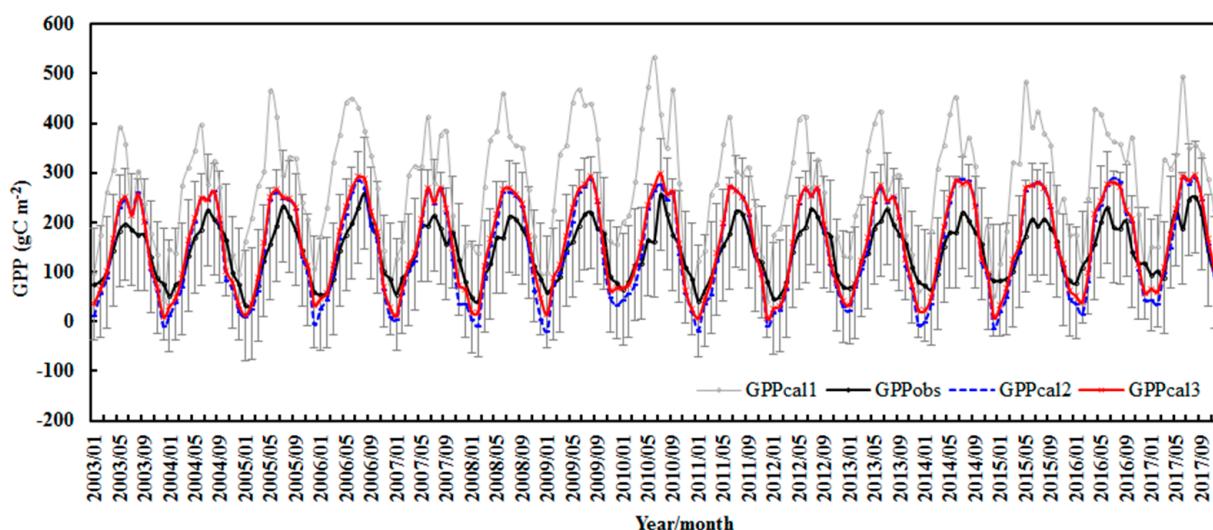


Figure 4. Observed and calculated monthly sums of GPP using the 2-factor EMGPP with coefficients at $S/Q < 0.5$ and $S/Q \geq 0.5$, and their combinations (GPP_{obs} , GPP_{cal1} , GPP_{cal2} , GPP_{cal3} , respectively) with error bars showing two times standard deviations of the observed GPPs from 2003–2017.

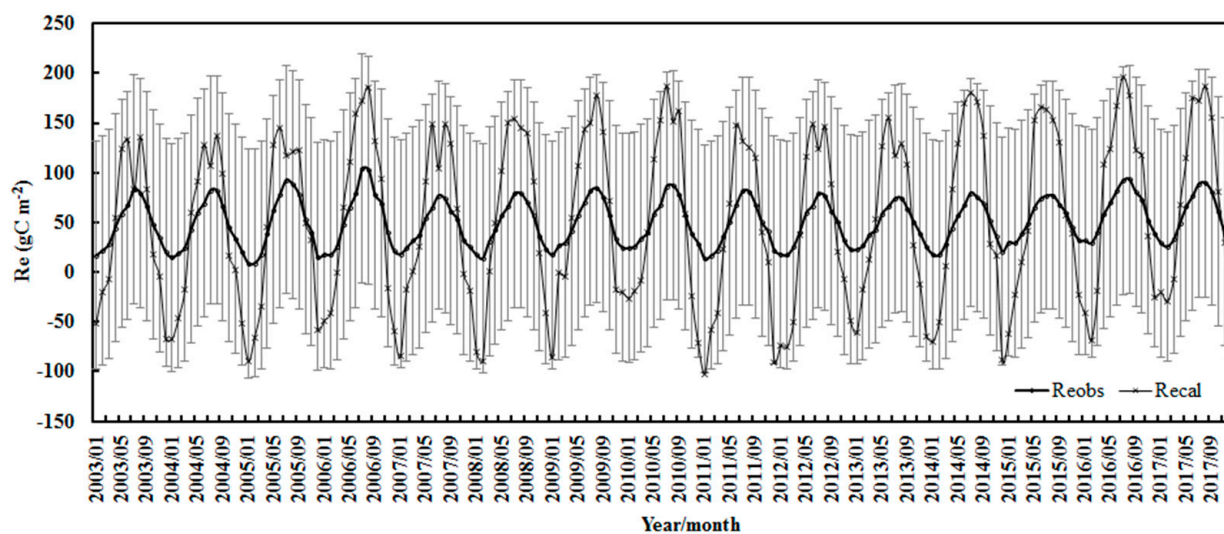


Figure 5. Observed and calculated monthly sums of respiration using the 2-factor EMRe (Re_{obs} and Re_{cal} , respectively), with error bars showing two times standard deviations of the observed respirations from 2003–2017.

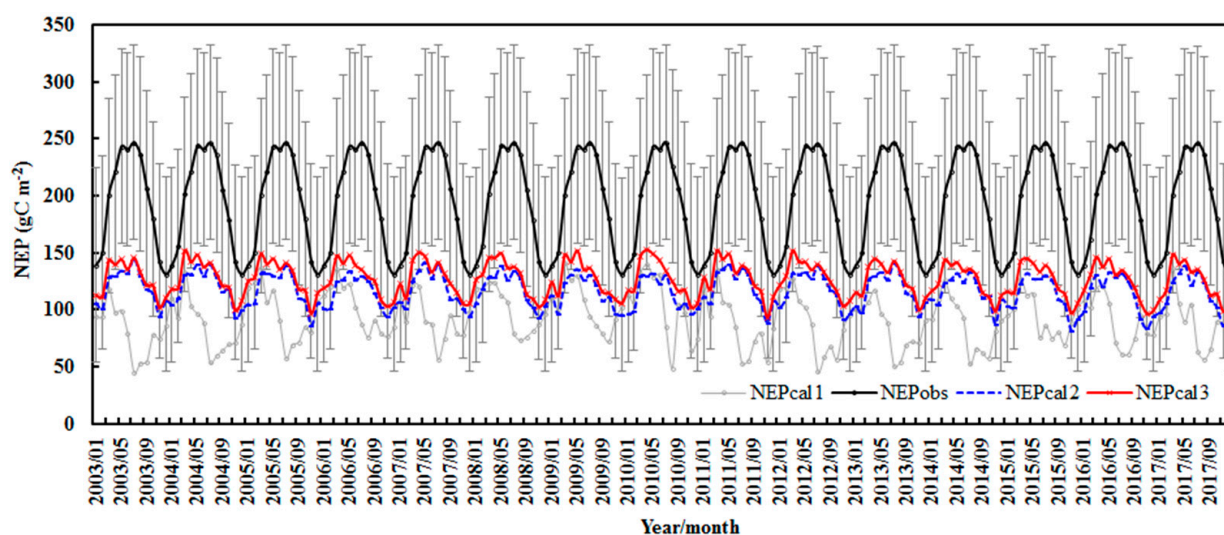


Figure 6. Observed and calculated monthly sums of NEPs using the 2-factor EMGPP with coefficients at $S/Q < 0.5$, $S/Q \geq 0.5$, and their combinations (NEP_{obs} , NEP_{cal1} , NEP_{cal2} , and NEP_{cal3} , respectively), with error bars showing two times standard deviations of the observed NEPs and EMRe from 2003–2017.

The EMRe overestimated the measured respirations by 5.52% in the averages from 2003–2017, but with a larger variation range. The EMNEP underestimated the NEPs by 52.71%, 40.09%, and 34.99%, respectively, for the three atmospheric conditions (clean, polluted, and realistic). Large differences also existed in NEP simulations such as GPP. The reasons were (1) more complicated processes happened in daytime and nighttime respirations and then influenced NEP; (2) both GPP and daytime respirations were influenced by PAR [40,41] and GPP was more sensitive to the changes in PAR than other factors (E , S/Q); (3) the observed PAR from 2003–2017 by the station may have large measurement errors, which may be the main reason. It can be speculated from the results that the simulations of monthly sums of Re , as well as NEP using EMRe and EMNEP and measured PAR by Bai's group, were in reasonable agreement with their observations from 2013–2016 [40,41]; (4) extreme positive and negative observed respirations were removed in the quality control, resulting in the small change ranges; (5) there were data gaps in the observations, but this

issue did not affect empirical model developments of EMGPP, EMRe, and EMNEP [40,41]; and (6) estimation errors in empirical models.

3.1.4. Annual Sum Simulations of GPP, Re, and NEP

The annual sum simulations of GPP, Re, and NEP were calculated and shown in Figures 7–9. Similar phenomena and estimates were also found for their annual sums as for the monthly sums. The mean annual ratios were 1.93, 1.04, and 1.11 for GPP_{cal}/GPP_{obs} under three atmospheric conditions from 2003–2017, respectively, 1.06 for Re_{cal}/Re_{obs} under the realistic atmospheric conditions, and 0.473, 0.599, and 0.650 for NEP_{cal}/NEP_{obs} under three atmospheric conditions. Thus, the empirical models also performed better simulations for Re (with a relative bias of 5.52%) and underestimated annual sums of NEP by 34.99% under realistic atmospheric conditions. The empirical models captured the peaks of GPP and Re in 2006, 2010, and 2016. The simulations of annual sums of NEP exhibited similar variations for polluted and realistic atmospheric conditions; the observed GPP and NEP in 2016 had some measurement problems, which are reflected by the simulations [40,41]. In general, the empirical models of GPP, Re, and NEP better reproduced their interannual variations.

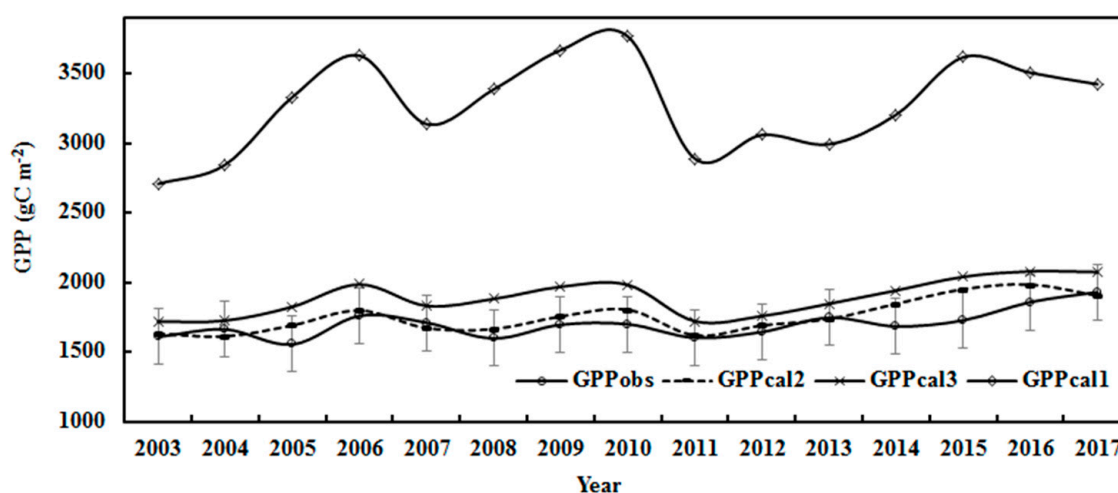


Figure 7. Observed and calculated annual sums of GPP using the 2-factor EMGPP with coefficients at $S/Q < 0.5$, $S/Q \geq 0.5$, and their combinations (GPP_{obs} , GPP_{cal1} , GPP_{cal2} , and GPP_{cal3} , respectively) with error bars showing two times standard deviations of the observed GPP from 2003–2017.

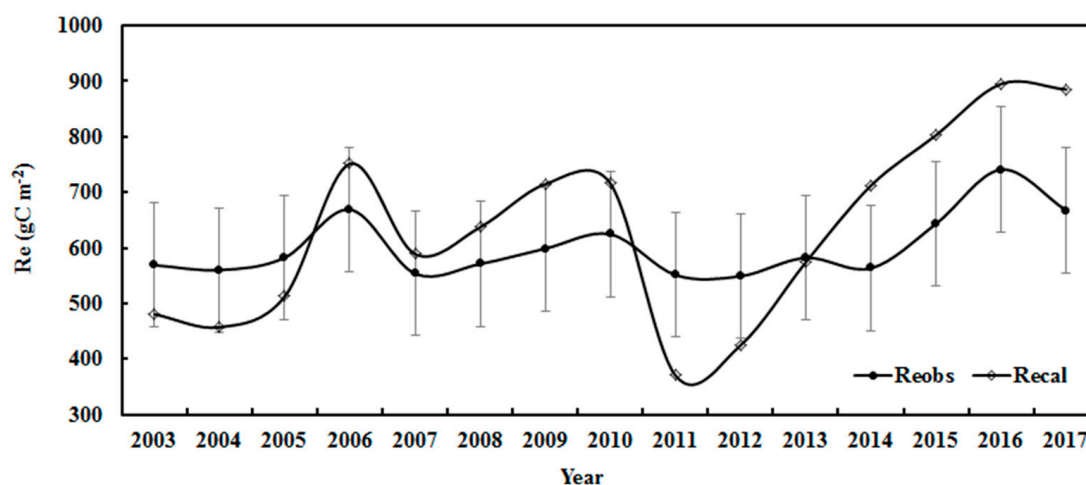


Figure 8. Observed and calculated annual sums of respiration using the 2-factor EMRe (Re_{obs} , Re_{cal}) with error bars showing two times standard deviations of the observed respirations from 2003–2017.

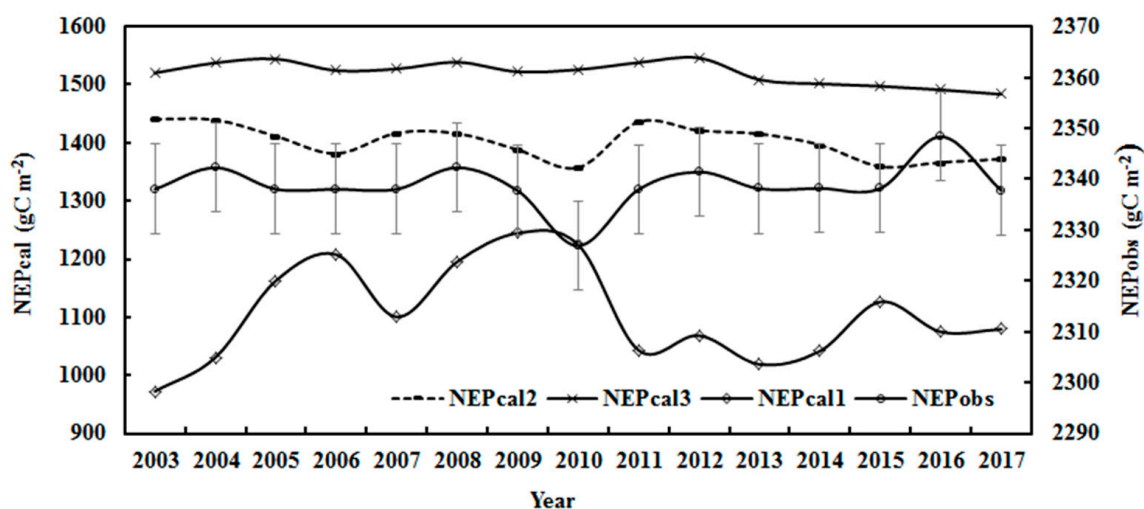


Figure 9. Observed and calculated annual sums of NEP using the 2-factor EMGPP with coefficients at $S/Q < 0.5$, $S/Q \geq 0.5$, and their combinations and EMRe with error bars showing two times standard deviations of the observed NEPs (NEP_{obs} , NEP_{cal1} , NEP_{cal2} , and NEP_{cal3} , respectively) from 2003–2017.

The ratio GPP_{cal}/GPP_{obs} of 1.93 and GPP decreases with the increase in S/Q (representative of all atmospheric GLPs) [40], which reveals that a clean atmosphere is more beneficial to large GPP production and storage in plants than a polluted atmosphere. A similar phenomenon is also reported where fire pollution causes a GPP reduction [83]. Therefore, we strongly recommend controlling the increase of all kinds of GLPs in the atmosphere (e.g., GHGs, as well as air pollutants, aerosols, and VOCs (volatile organic compounds)) so as to mitigate climate warming. In the future, with the extensive implementation of the afforestation strategy in China and other countries in the world, more and more BVOCs will be emitted from vegetation, resulting in fast increases of ozone, secondary organic aerosols (SOA), and other new GLPs, i.e., the increases of atmospheric GLPs [65,84–86]. So, a stronger control of GLP emissions and production than before is suggested. This point of view is supported by a study that a clear positive and non-linear relationship exists between air temperature and total atmospheric GLPs for some representative stations, Qianyanzhou, Ankara ($39^{\circ}58'21.7''$ N, $32^{\circ}51'49.3''$ E), Sodankylä (67.367 N, 26.630 E) in the Arctic, and Dome C ($75^{\circ}06'$ S, $123^{\circ}21'$ E) in the Antarctic, indicating an important mechanism that air temperature will decrease with the decrease of all types of chemical compositions in the atmosphere [87].

3.1.5. Long-Term Variations of Annual Sums of GPP, Re, and NEP

Under all sky conditions (i.e., realistic atmospheric conditions) from 2003–2017, the simulated and observed annual sums of GPP increased by 1.04% and 0.93%, respectively. Similarly, the estimated and observed annual sums of Re increased by 4.57% and 1.06%, respectively, whereas the computed and observed annual sums of NEP decreased by 0.18% and 0.01%, respectively. Considering $NEE = -NEP$, the calculated and observed annual sums of NEE increased by 0.18% and 0.01%, respectively, indicating that a carbon sink increased in the Qianyanzhou subtropical coniferous forest from 2003–2017. The above results manifested that a carbon sink increased in the Qianyanzhou subtropical coniferous forest from 1985 to 2017. Though annual sums of NEP were underestimated, similar long-term variations were found for the simulated and observed NEP. In addition, long-term variations of the simulations of GPP and Re were in agreement with their measurements.

As for the long-term variations of driving factors of GPP, RE, and NEP, annual averages of PAR and air temperature in 2003–2017 decreased by 0.28% and 0.02% (corresponding to 0.06°C), respectively, and annual mean water vapor pressure increased by 0.87% (Figure 10). Therefore, the increase in water supply (e.g., precipitation, soil moisture, vapour pressure

deficit, and canopy water content) contributed to the increases in the calculated and observed annual sums of GPP and Re [40,88–90]. It is known that many factors (light, T, RH, water, O₂, and CO₂ concentrations, etc.) control the processes of GPP, Re, and NEP, and the PAR energy controls the main processes and the interactions between GPP, Re, NEP, and their other driving factors (e.g., T, RH, and E) through different ways and mechanisms in the atmosphere, plants, and soil. PAR energy balance at the canopy level can capture and describe these multiple and dynamic interactions from the hourly to annual time scales, and some detailed mechanisms of PAR use are reported in papers [40,41] and this study. Therefore, the positive and negative responses of GPP, Re, and NEP to their driving factors are easier and much more accurate to be determined using the PAR energy method than each single-direction specific process studying method.

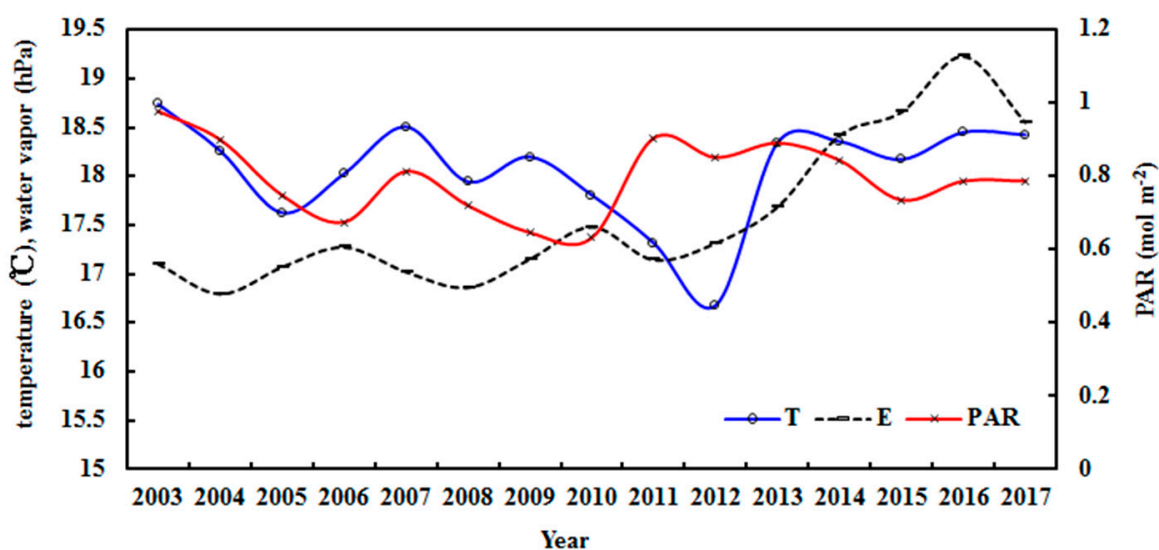


Figure 10. Annual averages of observed air temperature (T) and water vapor pressure (E), and hourly sums of observed PAR from 2003–2017.

3.2. Relations between GPP and SIF and Its Application to Calculate GPP

The strong relationships (most linear) between GPP and satellite SIF are found in various forests and can be used to estimate GPP [91–96]. For example, the square of the correlation coefficient (R^2) is in the range of 0.62–0.92 in evergreen forests [91]. The relationships between GPP and SIF were studied using the calculated monthly GPP (GPP_{cal1} , GPP_{cal2} , and GPP_{cal3} , representing relatively clean, realistic, and polluted atmospheric conditions, respectively) and monthly SIF at this subtropical coniferous forest. Firstly, strong linear correlations were found (Figure 11). Stronger correlations were obtained between GPP_{cal2} , GPP_{cal3} , and SIF ($R^2 = 0.912, 0.900$) than between GPP_{cal1} and SIF ($R^2 = 0.599$), indicating that better correlations existed between GPP and SIF for realistic and polluted atmospheric conditions, revealing that (1) the representative atmosphere in this subtropical coniferous forest was the atmospheric conditions at $S/Q \geq 0.5$, and the atmosphere had very high GLP loads (more aerosols, clouds, misty, etc.). For example, the hourly average of S/Q was 0.85 from May 2013 to December 2016 [40]; (2) the estimated GPP and satellite SIF have better temporal and spatial consistency under realistic and polluted atmospheric conditions.

In addition, the linear correlation between the observed monthly GPP and monthly SIF was 0.8460, which was lower than that between GPP_{cal2} , GPP_{cal3} , and SIF, indicating that the calculated GPP (GPP_{cal2} , GPP_{cal3}) using EMGPP can provide more reasonable estimates of GPP, as the SIF was derived from another independent data source, and some advantages to solve unavoidable shortages in GPP measurements (e.g., in 2016) [40].

Secondly, larger correlations were found for non-linear correlations between calculated monthly GPP and monthly SIF (Figure 12). R^2 was 0.618, 0.915, and 0.914 between GPP_{cal1} ,

GPP_{cal2}, GPP_{cal3}, and SIF. Similarly, higher non-linear correlations were also obtained between GPP_{cal2}, GPP_{cal3}, and SIF than those between GPP_{cal1} and SIF.

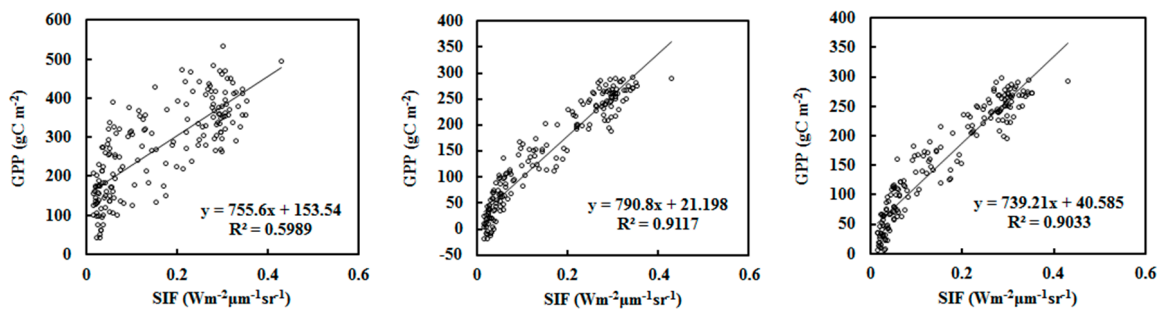


Figure 11. Relationships between the estimated monthly sums of GPP (GPP_{cal1}, GPP_{cal2}, GPP_{cal3}, **left**, **middle**, and **right**) and monthly mean solar-induced chlorophyll fluorescence (SIF) from 2003–2017. The lines show linear fits to the data for GPP and SIF.

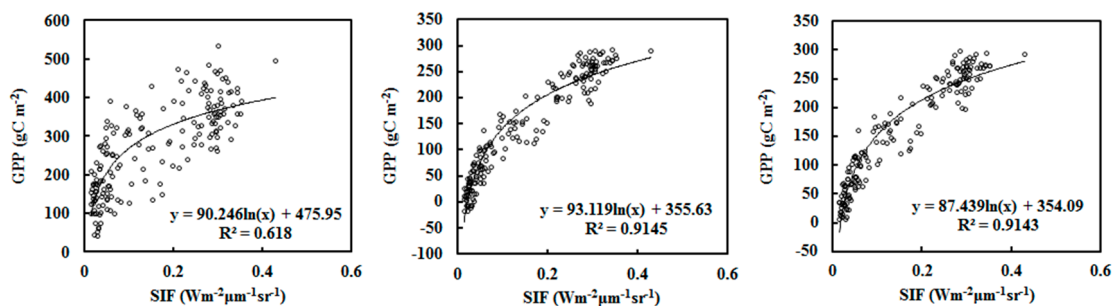


Figure 12. Relationships between the estimated monthly sums of GPP (GPP_{cal1}, GPP_{cal2}, GPP_{cal3}, **left**, **middle**, and **right**) and monthly mean solar-induced chlorophyll fluorescence (SIF) from 2003–2017. The lines show non-linear fits to the data for GPP and SIF.

The R² values between the observed monthly GPP and monthly SIF were 0.895 for the non-linear relationship and 0.846 for the linear relationship. These values were smaller than the corresponding R² between GPP_{cal2}, GPP_{cal3}, and SIF. This indicates that the non-linear GPP/SIF can better describe the inherent interactions associated with the processes of GPP and SIF than the linear GPP/SIF.

Using Equations (4) and (5) determined by linear and non-linear fitting of the monthly estimated GPP (GPP_{cal3 1}, and GPP_{cal3 n}) and the monthly SIF, the monthly sums of GPP were calculated (Figure 13). Generally, the GPP estimates were in reasonable agreement with those calculated using EMGPP. The ratio of GPP_{cal3 1}/SIF was 1.29 (range from 0.52–10.16), and GPP_{cal3 n}/SIF was 1.07 (−1.97–7.61). The estimated GPP using GPP/SIF and EMGPP methods can better reproduce the seasonal variations in GPP. Their GPP simulations with the larger ratios appeared in winter seasons (December and January), and this was mainly caused by low GPP.

$$GPP = 739.21 \times SIF + 40.585 \quad (R^2 = 0.903) \quad (4)$$

$$GPP = 87.439 \times \ln(SIF) + 354.09 \quad (R^2 = 0.914) \quad (5)$$

where GPP and SIF are the monthly sums of GPP and monthly mean SIF, respectively.

Furthermore, the annual sums of GPP were also obtained, and both simulation performances were significantly improved. The relative errors were 5.20% (0–15.33%) and 4.88% (0.15–13.23%) when using linear and non-linear Equations (1) and (2), respectively. Therefore, both GPP/SIF methods captured the annual sums of GPP and can be used as an additional tool, and the non-linear GPP/SIF method showed a slightly better performance than the linear method (for monthly and annual GPP). It was due to GPP_{cal3 1}/SIF or

GPP_{cal31} providing a more detailed description of the direct and diffuse PAR roles related to canopy structure, while the EMGPP expressed the multiple interactions between PAR and absorbing and scattering GLPs, and the reflections between canopy, land, and the atmosphere from sunrise to sunset [40]. However, most of the SIF obtained by popular methods were limited to these important factors that were not well-described, as many factors affect the accurate SIF quantification contributed by the whole canopy, e.g., observation angle, light absorption, multiple light scattering, and canopy structure [91,95–99]. It should also be noted that the non-linear relationship better revealed the inherent connections between the low GPP and low SIF, corresponding to the winter season and low solar zenith angle during the day. Under these specific conditions, the diffuse radiation and high atmospheric GLPs play significant roles in GPP, which can be seen from the sensitivity tests using EMGPP and larger GPP changes with the change in S/Q (representing atmospheric GLPs) at high S/Q levels compared to that at low S/Q [40]. The hourly processes of GPP, light absorption, and scattering (i.e., the GPP, photochemical, and scattering terms) in the atmosphere, as well as the canopy, are described in empirical models of GPP, Re, and NEP, especially using the optical air mass to describe the optical length and its hourly changes from sunrise to sunset. All of these calculations describe the light distributions of absorption and scattering under all sky conditions [40,41]. The above non-linear relationship was mainly caused by PAR transferring in relative curve lines in the realistic atmosphere, especially around the early morning and late afternoon.

The long-term variations of the annual sums of GPP and annual mean SIF from 2003–2017 were investigated. They shared a similar increase trend of 2.00%, 1.97%, and 1.04% per year for the calculated GPP_{cal31} , GPP_{cal3n} , and GPP_{cal3} , respectively, and 0.93% for GPP_{obs} . The increase in GPP was mainly caused by the increase in water vapor (0.87% per year), which was consistent with the sensitivity analyses using EMGPP. GPP increases/decreases with the decrease/increase in PAR and GPP increases/decreases with the increase/decrease in water vapor [40]. The annual mean PAR and air temperature were decreased by 0.30% and 0.02% per year from 2003–2017, respectively. It is reported that global solar radiation decreased at JiAn city (~20 km away from the Qianyanzhou station) from 2003–2015 [100].

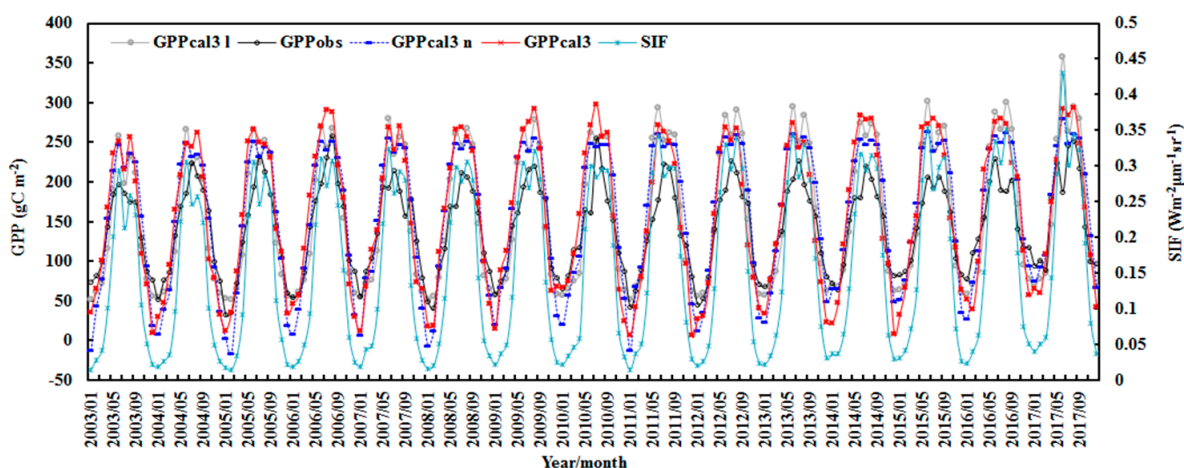


Figure 13. Monthly sums of GPP calculated using EMGPP (GPP_{cal3}) and GPP/SIF linear and non-linear relations (GPP_{cal31} and GPP_{cal3n}), observed GPP (GPP_{obs}), and SIF from 2003–2017.

4. Discussion

4.1. Possible Reasons for the Underestimations of NEP

More detailed analyses for the underestimations of NEP are provided here. The GPP and Re simulations from 2003–2017 and 2013–2016 using the measured dataset of solar radiation and meteorology [40] (Bai’s group) exhibited good reproducibility, but a larger variation ranges more for Re estimates than the observations. This discrepancy

might be due to the data processing of screening out extreme positive and negative Re values [41,67,69,101]. It was slightly strange for the larger underestimations of NEPs from 2003–2017, compared to the overestimations of NEPs from 2013–2016 [40,41]. It may be caused by the calculation of $NEP = GPP - Re$, positive and negative Re values during a day, and too many factors affect respiration processes, e.g., PAR, T, RH, E, etc. In addition, the measurements of PAR may be an important reason because GPP (as well as Re and NEP) is most sensitive to the changes in PAR [40], but the solar radiation sensors on the platform in the flux tower are very difficult to keep daily cleaning, maintenance, horizontal levels, and regular calibration from 2003–2017. For example, the PAR sensor was attenuated annually by about 3.6% [73]. In contrast, the NEP simulations from 2013–2016 provided reasonable overestimates as GPP and NEP simulations using the newly calibrated solar radiation sensors and making timely cleaning and maintenance [70].

The PAR comparison was performed between the measurements from the PAR sensors of the Qianyanzhou station and another set of solar radiation systems (Bai's group, described as PAR_{QYZ} , PAR_B , respectively) from May 2013 to December 2016. As shown in Figure 14, two PAR observations varied in similar patterns generally, but monthly PAR_B values were a little larger than PAR_{QYZ} , indicating that the PAR sensor at the Qianyanzhou station requires calibration and timely maintenance. Additionally, it is suggested that the PAR sensor can also be timely calibrated using a new calibration method described in [102] for high-quality observations of solar radiation at this station. Regular and timely calibration and maintenance of solar radiation sensors on flux tower platforms in other locations worldwide are recommended. This will ensure accurate estimation of carbon exchange using reliable station measurement data and a variety of models.

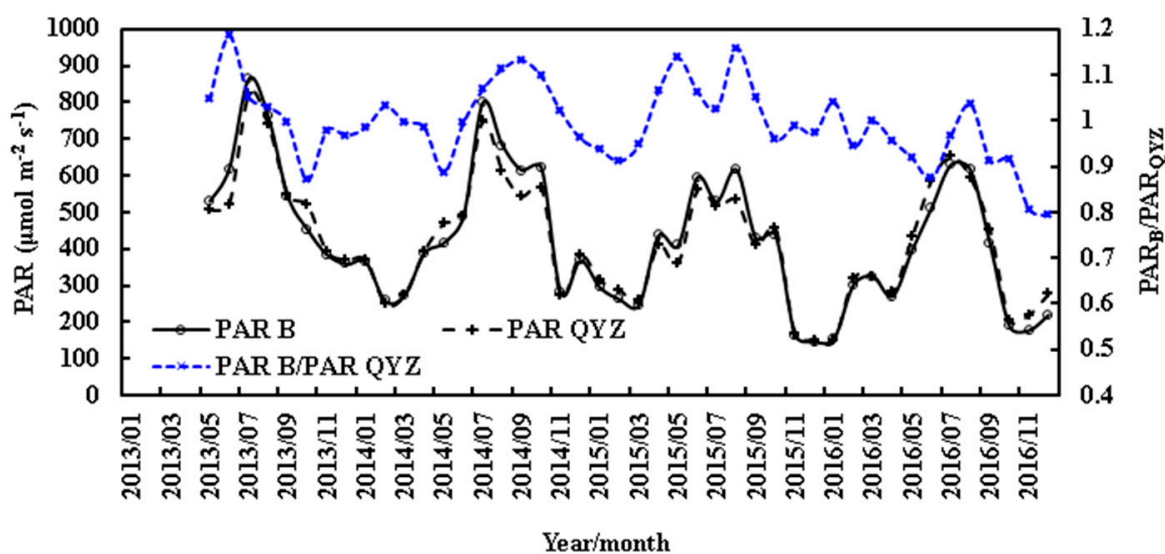


Figure 14. Monthly sums of PAR were measured using PAR sensors of Qianyanzhaou station and Bai's group (PAR_{QYZ} and PAR_B , respectively).

The empirical model of global solar radiation was developed using the hourly observed data (solar radiation and meteorology) from 2008–2011 at the Sodankylä station in the Antarctic and then applied to estimate global solar radiation from 2000–2018. Generally, reasonable performance was obtained [5]. A similar empirical model of Q was also developed using the hourly observed data from 2008–2011, and a little better performance from 2006–2016 was exhibited at the Dome C station in the Arctic [5]. These results indicated that the accurately observed solar radiation and strict routine maintenance of the solar sensors (e.g., Baseline Surface Radiation Network (BSRN) protocols) are very important to model development and, especially, model applications. Therefore, it is very necessary to conduct strict routine maintenance and timely calibration of the solar sensors and replace the broken solar sensors. Considering solar radiation (visible/PAR, Q, etc.), it is the basic

and significant energy to the atmosphere, vegetation, hydrosphere, and land. Together with their interactions, reliable and long-term measurements of solar radiation are extremely important in China and the globe.

More and recent long-term measurements using eddy covariance to quantify GPP, Re, and NEP/NEE are still very significant and useful (e.g., in Africa from 2010–2022) [103], so as to systemically and accurately understand and evaluate carbon exchange in China and the world.

4.2. Applications Potential of Empirical Models of GPP, Re, and NEP

There are more potential applications of empirical models of GPP, Re, and NEP in the future; for example, good relationships between the calculated GPP and satellite SIF were found and used to compute GPP as another method with large space coverage and better GPP and Re simulations from 2003–2017 and 2013–2016. From the simulations of GPP, Re, and NEP from 2013–2016 to 2003–2017, empirical models displayed reasonable performance from the hourly to daily, monthly, and annual time scales. PAR energy method showed potential advantages to deal with the multiple and complex interactions in the processes associated with CO₂ balance and is recommended to be further studied. PAR transfers in the atmosphere and PAR balance above a canopy level can objectively describe PAR absorption and scattering caused by atmospheric GLPs (including CO₂) ([40,41], and this study). Thus, the transformation/application of PAR balance to the empirical models of GPP, Re, and NEP exhibited acceptable short-term and long-term simulations (e.g., 2013–2016 and 2003–2017). The system of PAR–atmosphere–biosphere–land should be studied as a whole, and the PAR balance is an objective and useful tool for studying CO₂ exchange.

We strongly suggest measuring direct and diffuse solar radiation at solar radiation monitoring stations in order to fully understand the scattering roles/mechanisms of GLPs in the CO₂ exchange processes associated with the ecosystem [40,41,102], such as diffuse PAR roles on GPP [83,104–108].

4.3. Further Application of Respiration Model

The EMGPP model (Equation (1) in [40]) is a further application of the PAR balance method by replacing isoprene (one dominant species of BVOCs) with GPP from an empirical model of BVOC emissions (EMBE [70]). All of the above empirical models were applied/transformed from the PAR balance equation:

$$\text{PAR} = C_1 e^{-a_1 \text{ISOm}} \times \cos(Z) + C_2 e^{-kWm} \times \cos(Z) + C_3 e^{-S/Q} + C_0 \quad (6)$$

The ratio $\text{PAR}_{\text{TOA}} / (C_1 + C_2 + C_3 + |C_0|)$ between the measured PAR (PAR_{TOA}) and the calculated PAR ($C_1 + C_2 + C_3 + |C_0|$) at the top of the atmosphere (TOA) can be used to calibrate the PAR sensor [102]. To further apply the principle of PAR balance, the Re (DR) model (Equation (3) in [41]) was developed to deal with an energy balance during nighttime. The ratio between $C_1 + |C_0|$ (the calculated total longwave radiation emitted by the atmosphere and the surface) and the calculated longwave radiation emitted by vegetation (using Stefan–Boltzmann law) can be used to calibrate longwave radiation sensors, and reasonable results were found [41]. The meaning of C_1 and C_0 is fully discussed in studies [70,102]. In brief, the energy balance method (i.e., PAR, longwave radiation) has shown reasonable simulations of BVOCs and carbon flux components (GPP, Re, and NEP), as well as the application potential in the calibration of longwave radiation sensors.

It should be noted that a newly purchased PAR sensor was used in the solar radiation system (Bai's group) at the Qianyanzhou station, and routine maintenance (sensor surface cleaning, horizontal keeping, etc.) was conducted every day to obtain reliable data [70]. To evaluate the performance of the PAR sensor, a similar PAR empirical model as Equation (6) without an isoprene term ($e^{-a_1 \text{ISOm}}$) was developed for relatively clear sky conditions, using monthly averages from May 2013–December 2016 ($n = 9$, mean $S/Q = 0.443$). The ratio of the mean PAR to visible radiation (400–700 nm) from 2013–2016 (measured by

Bai's group) was 4.97 mol MJ^{-1} ($n = 9$). The relative bias between the summation of all coefficients and PAR_{TOA} (530.5 W m^{-2}) was 8.47%. It indicated that the PAR sensor had better stability from 2013–2016 under careful daily maintenance [70,102], and PAR data were reliable in the use of empirical model development and further application in GPP, Re, and NEP in the Qianyanzhou subtropical forest region.

4.4. Empirical Models of GPP, Re, and NEP

Empirical models of GPP, Re, and NEP captured their basic features, which were in agreement with other studies. In addition, these models describe dynamic and multiple-direction interactions in energy and especially quantify the relationships between energy (PAR) and atmospheric GLPs (CO_2 and other GLPs). The complex and interacted CO_2 processes in the atmosphere, biosphere, and land were described using PAR and its related components (e.g., diffuse PAR). It is an advantage that these empirical models can simplify CO_2 processes and capture the main properties of CO_2 without spending much time on specific processes. In the future, to obtain more accurate simulations of seasonal NEP, more studies are still needed, such as the improvement of measured PAR data quality and the timely calibration of PAR sensors. It should be emphasized that the energy interactions between photons, CO_2 molecules, and other GLP quantum obey the statistical law.

An inherent relation exists between E, T, and RH. Compared to T and RH, water vapor and/or E (as a representative of T and RH) play more vital and objective roles in the multiple processes and mechanisms (e.g., chloroplasts absorb the incoming PAR to convert CO_2 and H_2O and decompose water into [H] and O_2) in the atmosphere–vegetation–land system, along with its transfer between the atmosphere, vegetation, and land system. Water vapor is also a vital participant in chemical and photochemical reactions (CPRs), associated with OH, BVOCs, and solar radiation [65,70]. Additionally, the key driving roles of T in GPP and BVOC emissions can be reflected by the water vapor factor (in the sensitivity tests in references [40,70]) to some extent. The most important issue is that (1) water is a dominant driving factor in plant growth and carbon production (e.g., GPP), which was displayed by a sensitivity analysis of GPP [40]; and (2) water vapor represents air temperature and humidity objectively [109].

The large variation ranges of the estimated monthly sums of Re and NEP, compared to their observations for periods from 2013–2016 [41] and 2003–2017, may reveal some problems in data processing. For example, spike detection, threshold (u^*_c) determination of nocturnal friction velocity (u^*), and gap filling had evident effects on annual NEE estimates [102]. Using the u^*_c criterion, >50% of night data are removed [102]. A large quantity of flux data removal may cause small changes in the variation range in observed Re and NEP. The ratios of the measured annual sum Re/GPP and NEE/GPP were 0.764 and 0.236, respectively, from 2013–2016 [40] and 0.744 and 0.256, respectively from 2003–2017, indicating the relative magnitudes of Re and NEP to GPP. Thus, more studies on appreciated data-processing methods are needed to provide high-quality flux data with more relatively reliable maxima (positive and negative).

Under all sky conditions from 2003–2017, the simulated and observed annual sums of GPP, Re, and NEE showed an increasing carbon sink (Section 3.1.5), which was in line with and contributed to a carbon sink from 1980 to 2019 in China [110]. Wu et al. (2013) reported that the carbon density and carbon storage in Taihe County (Qianyanzhou located in Taihe County) increased from 1985–2003 [111].

From 2003–2017, the estimated and observed annual sums increased by 1.04% and 0.93%, respectively, for GPP, 4.57% and 1.06% for Re, and 0.18% and 0.01% for NEE, i.e., the estimates of GPP, Re, and NEE showed larger increase rates than the observations, revealing that the simulated GPP, Re, and NEE have larger enhanced carbon sink under realistic sky conditions than the measurements. It should be noted that the estimations of GPP, Re, and NEE obtained using continuous measurements of solar radiation and meteorological parameters at the Qianyanzhou station were more reliable than the observations, in which such data were removed by several methods in data processing [101]. Meanwhile, the

better and consistent performances (overestimations) of GPP, Re, and NEP (especially NEP) from 2013–2016, using the observation data of Bai's group, provided reasonable simulations of GPP, Re, and NEP [40,41]. Additionally, the solar radiation sensors were calibrated, and a HOBO weather station was newly bought before the measurement in the Qianyanzhou station from 2013–2016.

It would be an advantage and enable much progress to develop a generalized empirical model of GPP, Re, and NEP in China, following the procedures such as EMBE development from fitting a typical forest (temperate forest, subtropical bamboo, and plantation) to a primary generalized EMBE for representative forests in China [70].

4.5. Some Issues Associated with the Empirical Models, GLPs, and Climate Warming

PAR direct absorption and indirect utilization are associated with NO_2^* , H_2O , OH , and $\text{BVOCs} + \text{OH} + \text{O}_3$ [112]. The photochemical term expresses PAR use by all kinds of GLPs. In empirical models of GPP, Re, and NEP, the multiple interactions between PAR and its related terms (photochemical, scattering, and GPP/Re term in previous studies instead of BVOC terms) and EMBE are fully reported [40,41,70,85].

The sensitivity displayed that the GPP increases with the decrease of S/Q (associating with the increase of scattered PAR by GLPs, including aerosols and clouds) [40], which was in line with other model studies and observations (the increased diffuse radiation due to aerosols brings an increase of GPP) [83,104–108,113–115]. Considering similar phenomena for respiration together, light-use efficiency (or the diffuse radiation associated with atmospheric GLPs), and how much direct and scattered PAR is fully utilized by vegetation play significant roles in plant growth, carbon storage, and model performances.

To comprehensively understand empirical model performance, the uncertainties in the measurements and model predictions are reported: 20%–50% for the EC measurements [55], 300–600 $\text{gC m}^{-2} \text{ year}^{-1}$ for annual sums of NEE at different forests [52], 12–32% for the annual NEE estimates [53], $\pm 32\%$ for annual NEE, Re, and GPP values [116], and 5–100% for annual NEP estimates using traditional ecological models [40,41,50–52].

PAR is the first important driving factor in BVOC emissions and CO_2 exchange processes [38–41]. Using the PAR balance principle, we applied the EMBE to empirical models of GPP, then Re and NEP. Generally, reasonable performances of the Re and NEP were displayed. The EMGPP, EMRe, and EMNEP are simple and time-saving, and fewer variables can be obtained from the stations. The revealed basic mechanisms (such as GPP, Re, and NEP/NEE, which increased with the increases in diffuse PAR) agreed with other model results [117,118]. It is an important progress that the EMRe during nighttime was used to calibrate the longwave radiation sensor. Therefore, the energy balance method and the empirical models (BVOCs, GPP, Re, and NEP) are useful tools and are recommended to be developed for a better understanding of the carbon balance in China and in the world [40,119,120]. By combining with the popular models (in the introduction), it is beneficial to avoid using too many assumptions and parameters, considering these processes that we have not realized and analyzed. But there is a limitation for these empirical models. They should be previously developed using reliable observational data (fluxes, solar radiation, and meteorology) before their applications.

Currently, large uncertainties still exist in CO_2 flux measurements and model estimates (e.g., an underestimated land carbon sink over some regions in China from 2010–2016) [95], and the related knowledge gaps remain [121]. It was a greening pattern from 2000–2017 worldwide, and China contributes about 25% of the global net increase [59]. With the progress in achieving carbon peaking and carbon neutrality in the future, long-term afforestation will be conducted. It is urgent and beneficial to accurately estimate GPP, Re, and NEP, along with BVOCs [40,119,120,122], and evaluate the total carbon balance/sink (including BVOCs) under different climate scenarios using the integrated methods, including the empirical models, widely used models (DGVMs, XGBoost, ANN, GEOS-Chem atmospheric transport model, atmospheric inversion model, etc.), and using tower and satellite data [40,41,100,123,124].

It is found that the increases in absorbing and scattering GLPs contribute to the enhanced losses of global solar radiation in the atmosphere. This energy can heat the atmosphere and increase the air temperature (i.e., regional climate warming), as well as weaken the airmass movements (e.g., wind speed). The phenomena and mechanisms are evidently displayed in the Antarctic and Arctic regions (Sodankylä and Dome C sites) and other sites, especially (1) in the Dome C station because it is the cleanest and driest atmosphere [5]; (2) the highest air temperature increase rate appeared in the winter and the lowest (or lower) in the summer in some sites in China [87], corresponding to the large losses of solar UV and visible (or PAR) radiation in winter [125]; and (3) the decreasing trend in precipitation in Beijing (bigger decrease in the city than in the suburbs) from 1961–2004 [125].

The more GLPs (including water and water vapor) in the atmosphere, the more absorption and scattering energy accumulation and use/release in the atmosphere, resulting in large changes in precipitation and atmospheric vertical and horizontal movements (related to natural disasters, e.g., rainstorm, flood, mud-rock flow, and wild wind) of the atmosphere. Therefore, it will have multiple-win effects to reduce GLPs (GHGs, non-GHGs, particles, etc.) emitted from the anthropogenic and natural sources into the atmosphere and produced through CPRs in the atmosphere on achieving carbon peak and neutralization, controlling air pollution, and mitigating climate warming and extreme weather disasters [5,88].

The most important issue should be emphasized that the synchronous and high-quality observational data in multiple fields, such as atmosphere, biosphere, hydrology, land, and solar radiation, are very necessary in the stations in China and the world [126], especially for empirical model development and evaluation, so as to comprehensively study the individual process and mechanism along with their integrated processes and mechanisms in above associated fields as a whole system.

5. Conclusions

GPP, Re, and NEP in a subtropical coniferous forest from 2003–2017 were calculated using the empirical models of GPP, Re, and NEP, previously developed using hourly observational data from 2013–2016. Their simulations from the hourly to the daily, monthly, and annual time scales were in reasonable agreement with the observations, and their seasonal variations were well captured. For the annual sums under all skies, the simulations overestimated the observations by 11.38% for GPP and 5.52% for Re, while they underestimated the observations by 34.99% for NEP. The mean annual ratios GPP_{cal1}/GPP_{obs} and GPP_{cal3}/GPP_{obs} were 1.93 and 1.04 under relatively clean and polluted atmospheric conditions from 2003–2017, indicating that the forest would store more CO₂ (about two times GPP) under a clean atmosphere than a polluted atmosphere, and the objectives of reducing air pollutants and achieving carbon neutrality have win–win effects.

Timely maintenance and the calibration of PAR sensors are necessary to obtain accurate PAR observational data, together with better simulations of GPP, Re, and NEP, especially NEP.

GPP, Re, and NEE exhibited clear and similar long-term variation trends under all sky conditions from 2003–2017. The calculated and observed annual sums increased by 1.04% and 0.93%, respectively, for GPP, 4.57% and 1.06% for Re, and 0.18% and 0.01% for NEE. The estimated and observed annual sums of NEP decreased by 0.18% and 0.01%, respectively. These results were consistent with the fact that a carbon sink was enhanced in this subtropical coniferous forest from 1985–2017. As for their driving factors, annual mean PAR and air temperature decreased by 0.28% and 0.02%, respectively, and annual mean water vapor pressure increased by 0.87%, demonstrating that the water vapor or water supply played significant roles in and contributed to the increases in GPP, Re, and NEE, i.e., the carbon sink.

Strong relationships (linear and non-linear) between the simulated monthly GPP and the satellite monthly SIF ($R^2 > 0.90$) under polluted and realistic atmospheric conditions

were found, revealing that the atmosphere in the Qianyanzhou coniferous forest was in high GLP loads. The linear and non-linear equations were used to calculate GPP from 2003–2017 with good performances. For annual sums of GPP, the relative biases were 5.20% and 4.88%, respectively, using linear and non-linear equations. It indicates that (1) the non-linear relationship displayed better performance than the linear, implying that a non-linear law existed in PAR transfer (associated with GPP and SIF) in the atmosphere; and (2) better simulations than the EMGPP with a relative bias of 11.38% for the annual sums of GPP were found. Later, similar increasing trends were also found for the calculated and the observed GPP. All these results demonstrated that satellite SIF and the method of GPP/SIF relation provide useful tools to calculate GPP over a large region.

Based on the simulations of GPP, Re, and NEP from 2013–2016 and 2003–2017, the PAR energy balance method and its transformations to the empirical models (GPP, Re, NEP, and BVOCs) can be used to study the processes of total carbon exchange (including BVOCs) and understand the multiple and dynamic interactions between atmospheric components (CO₂ and other GLPs through absorption and scattering) and PAR in this subtropical forest, and it is deserved for further development and applications in other forests. Several studies supported that reduced atmospheric substances (i.e., a cleaner atmosphere) are beneficial to more carbon stored in the plants, a clean atmosphere, and slowing down climate warming. Thus, it is recommended to reduce the atmospheric GLPs through the control of direct emissions and secondary formations via CPRs.

Author Contributions: Conceptualization, J.B.; methodology, J.B.; validation, J.B.; formal analysis, J.B.; investigation, J.B.; resources, F.Y., H.W., M.X. and L.Y.; writing—original draft preparation, J.B.; writing—review and editing, J.B., F.Y., H.W., M.X. and L.Y.; funding acquisition, J.B. All authors have read and agreed to the published version of the manuscript.

Funding: This research was funded by the National key R&D program (No. 2021YFE0118000), ESA-MOST China Dragon Cooperation, Dragon 4 and 5 projects (ID 32771, ID 59013), National Natural Science Foundation of China (No. 41275137), and the Special Project on National Science and Technology Basic Resources Investigation of China (2021FY100701).

Data Availability Statement: Data available on request due to restrictions privacy. The data that support the findings of this study are available on request from the corresponding author. Some datasets for this study will be available in a Big Earth Data Platform for Three Poles, <http://poles.tpdc.ac.cn/zh-hans/> (accessed on 1 October 2024).

Acknowledgments: The authors thank all the people for their great assistance, including A. Guenther at the Department of Earth System Science, University of California, Irvine, USA, Andrew Turnipseed at 2B Technologies, Inc. Boulder, USA, J. Greenberg at National Center for Atmospheric Research, Boulder, USA, T. Duhl at Tufts University, USA; G.R. Yu, Q.K. Li, G.Z. Liu, L. Huang, Y.G. Wang, S.Y. Yin, J.D. Zou, J.Z. Zhang, Y.F. Huang, G.L. Zhu at Qianyanzhou Experimental Station of Red Soil and Hilly Land, CAS, X.W. Wan, Y.M. Wu, and H.T. Liu at the Institute of Atmospheric Physics, CAS. The authors thank the Qianyanzhou Experimental Station for providing meteorological and solar radiation, as well as carbon flux data from 2003–2017. The authors also thank J.F. Xiao and X. Li for providing the SIF product that can be obtained from the GOSIF website (<https://globalecology.unh.edu/data/GOSIF.html>, accessed on 1 October 2024).

Conflicts of Interest: The authors declare no conflicts of interest.

Abbreviations

ANN	Artificial neural networks
BVOCs	Biogenic volatile organic compounds
CPRs	Chemical and photochemical reactions
DGVMs	Dynamic global vegetation models
EC	Eddy covariance
EMGPP, EMRe, EMNEP	Empirical models of GPP, Re, and NEP
GHG	Greenhouse gas

GIS	Geographic information system
GLP	Gas, liquid, and particle
GPP	Gross primary production
GOSIF	Multi-source-driven SIF product
MAD	Mean absolute deviations
MERRA-2	Modern-Era Retrospective Analysis for Research and Applications
MODIS	Moderate Resolution Imaging Spectroradiometer
NEE	Net ecosystem exchange
NEP	Net ecosystem productivity
NMSE	Normalized mean-square error
OCO-2	Orbiting Carbon Observatory-2
PAR	Photosynthetically active radiation
RE	Respiration
RMSE	Root mean-square errors
SIF	Satellite solar-induced fluorescence
SOA	Secondary organic aerosols
VOCs	Volatile organic compounds
XGBoost	Extreme gradient boosting
Q	Solar global radiation
D	Solar direct radiation
S	Solar diffuse radiation
T	Temperature
RH	Relative humidity
E	Water vapor pressure
R ²	Coefficient of determination

References

1. Vaughan, D.G.; Marshall, G.J.; Connolley, W.M.; King, J.C.; Mulvaney, R. Climate Change: Devil in the Detail. *Science* **2001**, *293*, 1777–1779. [[CrossRef](#)] [[PubMed](#)]
2. Vaughan, D.G.; Marshall, G.J.; Connolley, W.M.; Parkinson, C.; Mulvaney, R.; Hodgson, D.A.; King, J.C.; Pudsey, C.J.; Turner, J. Recent rapid regional climate warming on the Antarctic Peninsula. *Clim. Chang.* **2003**, *60*, 243–274. [[CrossRef](#)]
3. Cohen, J.; Screen, J.A.; Furtado, J.C.; Barlow, M.; Whittleston, D.; Coumou, D.; Francis, J.; Dethloff, K.; Entekhabi, D.; Overland, J.; et al. Recent Arctic amplification and extreme mid-latitude weather. *Nat. Geosci.* **2014**, *7*, 627–637. [[CrossRef](#)]
4. Turner, J.; Lu, H.; White, I.; King, J.C.; Phillips, T.; Hosking, J.S.; Bracegirdle, T.; Marshall, G.J.; Mulvaney, R.; Deb, P. Absence of 21st century warming on Antarctic Peninsula consistent with natural variability. *Nature* **2016**, *535*, 411–415. [[CrossRef](#)]
5. Bai, J.; Zong, X.; Ma, Y.; Wang, B.; Zhao, C.; Yang, Y.; Guang, J.; Cong, Z.; Li, K.; Song, T. Long-term variations in global solar radiation and its interaction with atmospheric substances at Qomolangma. *Int. J. Environ. Res. Public Health* **2022**, *19*, 8906. [[CrossRef](#)]
6. Zavalishin, N.N. Reasons for Modern Warming: Hypotheses and Facts. *J. Atmos. Sci. Res.* **2021**, *5*, 11–17. [[CrossRef](#)]
7. Ahmed, M.; Khan, A.M.; Bibi, S.; Zakaria, M. Convergence of per capita CO₂ emissions across the globe: Insights via wavelet analysis. *Renew Sustain Energy Rev.* **2017**, *75*, 86–97. [[CrossRef](#)]
8. Stocker, T.; Qin, D.W.; Plattner, G.K.; Tignor, M.; Allen, S.K.; Boschung, J.; Nauels, A.; Xia, Y.; Bex, V.; Midgley, P.M.; et al. (Eds.) IPCC 2013: Summary for Policymakers. In *Climate Change 2013: The Physical Science Basis. Contribution of Working Group I to the Fifth Assessment Report of the Intergovernmental Panel on Climate Change*; Cambridge University Press: Cambridge, UK; New York, NY, USA, 2013.
9. Stips, A.; Macias, D.; Coughlan, C.; Garcia-Gorriz, E.; Liang, X.S. On the causal structure between CO₂ and global temperature. *Sci. Rep.* **2016**, *6*, 21691. [[CrossRef](#)]
10. Gurney, K.R.; Law, R.M.; Denning, A.S.; Rayner, P.J.; Baker, D.; Bousquet, P.; Bruhwiler, L.; Chen, Y.-H.; Ciais, P.; Fan, S.; et al. Towards robust regional estimates of CO₂ sources and sinks using atmospheric transport models. *Nature* **2002**, *415*, 626–630. [[CrossRef](#)]
11. Wofsy, S.C.; Goulden, M.L.; Munger, J.W.; Fan, S.M.; Bakwin, P.S.; Daube, B.C.; Bassow, S.L.; Bazzaz, F.A. Net exchange of CO₂ in a midlatitude forest. *Science* **1993**, *260*, 1314–1317. [[CrossRef](#)]
12. Baldocchi, D.; Falge, E.; Gu, L.; Olson, R.; Hollinger, D.; Running, S.; Anthoni, P.; Bernhofer, C.; Davis, K.; Evans, R.; et al. FLUXNET: A new tool to study the temporal and spatial variability of ecosystem-scale carbon dioxide, water vapor, and energy flux densities. *Bull. Am. Meteorol. Soc.* **2001**, *82*, 2415–2434. [[CrossRef](#)]
13. Baldocchi, D. How eddy covariance flux measurements have contributed to our understanding of global change biology. *Glob. Chang. Biol.* **2020**, *26*, 242–260. [[CrossRef](#)] [[PubMed](#)]

14. Yamamoto, S.; Saigusa, N.; Gamo, M.; Fujinuma, Y.; Inoue, G.; Hirano, T. Findings through the AsiaFlux network and a view toward the future. *J. Geogr. Sci.* **2005**, *15*, 142–148. [[CrossRef](#)]
15. Goulden, M.; Winston, G.; Cmillan, A.S.M.; Litvak, M.; Read, E.; Rocha, A.; Robelliot, J. An eddy covariance mesonet to measure the effect of forest age on land–atmosphere exchange. *Glob. Chang. Biol.* **2006**, *12*, 2146–2162. [[CrossRef](#)]
16. Foken, T.; Aubinet, M.; Leuning, R. The eddy covariance method. In *Eddy Covariance: A Practical Guide to Measurement and Data Analysis*; Aubinet, M., Vesala, T., Papale, D., Eds.; Springer Atmospheric Sciences: Berlin/Heidelberg, Germany, 2012; pp. 1–19.
17. Yao, J.Y.; Gao, Z.M.; Huang, J.P.; Liu, H.P.; Wang, G.Y. Technical note: Uncertainties in eddy covariance CO₂ fluxes in a semiarid sagebrush ecosystem caused by gap-filling approaches. *Atmos. Chem. Phys.* **2021**, *21*, 15589–15603. [[CrossRef](#)]
18. Klosterhalfen, A.; Chi, J.; Kljun, N.; Lindroth, A.; Laudon, H.; Nilsson, M.B.; Peichl, M. Two-level eddy covariance measurements reduce bias in land-atmosphere exchange estimates over a heterogeneous boreal forest landscape. *Agric. For. Meteorol.* **2023**, *339*, 109523. [[CrossRef](#)]
19. Liu, S.; Feng, Z.; Fang, S.; Liu, G.; Yuan, X.; Shang, B.; Xu, Y.S.; Fu, H.W.; Jin, Z.P.; Chen, Z.Y.; et al. Assessing the accuracy of eddy-covariance measurement at different source emission scenarios. *J. Geophys. Res. Atmos.* **2024**, *129*, e2023JD040701. [[CrossRef](#)]
20. Van de Boer, A.; Moene, A.F.; Schuttemeyer, D.; Graf, A. Sensitivity and uncertainty of analytical footprint models according to a combined natural tracer and ensemble approach. *Agric. For. Meteorol.* **2013**, *169*, 1–11. [[CrossRef](#)]
21. Lee, X. On micrometeorological observations of surface-air exchange over tall vegetation. *Agric. For. Meteorol.* **1998**, *91*, 39–49. [[CrossRef](#)]
22. Finnigan, J.J.; Clement, R.; Malhi, Y.; Leuning, R.; Cleugh, H. A re-evaluation of long-term flux measurement techniques part I: Averaging and coordinate rotation. *Bound.-Layer Meteorol.* **2003**, *107*, 1–48. [[CrossRef](#)]
23. Twine, T.; Kustas, W.; Norman, J.; Cook, D.; Houser, P.; Meyers, T.; Prueger, J.; Starks, P.; Wesely, M. Correcting eddy-covariance flux underestimates over a grassland. *Agric. For. Meteorol.* **2000**, *103*, 27–300. [[CrossRef](#)]
24. Foken, T. The energy balance closure problem: An overview. *Ecol. Appl.* **2008**, *18*, 1351–1367. [[CrossRef](#)] [[PubMed](#)]
25. Zhou, Y.; Li, D.; Li, X. The effects of surface heterogeneity scale on the flux imbalance under free convection. *J. Geophys. Res. Atmos.* **2019**, *124*, 8424–8448. [[CrossRef](#)]
26. Cao, M.K.; Prince, S.D.; Li, K.R.; Tao, B.; Small, J.; Shao, X.M. Response of terrestrial carbon uptake to climate interannual variability in China. *Glob. Chang. Biol.* **2003**, *9*, 536–546. [[CrossRef](#)]
27. Cao, M.K.; Tao, B.; Li, K.R.; Shao, X.M.; Prience, S.D. Interannual variation in terrestrial ecosystem carbon fluxes in China from 1981 to 1998. *Acta Bot. Sin.* **2003**, *45*, 552–560.
28. Zeng, N.; Mariotti, A.; Wetzal, P. Terrestrial mechanisms of interannual CO₂ variability. *Glob. Biogeochem. Cycles* **2005**, *19*, Gb1016. [[CrossRef](#)]
29. Friedlingstein, P.; Cox, P.; Betts, R.; Bopp, L.; Von Bloh, W.; Brovkin, V.; Cadule, P.; Doney, S.; Eby, M.; Fung, I.; et al. Climate-carbon cycle feedback analysis: Results from the (CMIP)-M-4 model intercomparison. *J. Clim.* **2006**, *19*, 3337–3353. [[CrossRef](#)]
30. Feng, X.; Liu, G.; Chen, J.M.; Chen, M.; Liu, J.; Ju, W.M.; Sun, R.; Zhou, W. Net primary productivity of China’s terrestrial ecosystems from a process model driven by remote sensing. *J. Environ. Manag.* **2007**, *85*, 563–573. [[CrossRef](#)]
31. Li, X.L.; Liang, S.L.; Yu, G.R.; Yuan, W.P.; Cheng, X.; Xia, J.Z.; Zhao, T.B.; Feng, J.M.; Ma, Z.G.; Ma, M.G.; et al. Estimation of gross primary production over the terrestrial ecosystems in China. *Ecol. Model.* **2013**, *261*, 80–92. [[CrossRef](#)]
32. Sitch, S.; Friedlingstein, P.; Gruber, N.; Jones, S.D.; Murray-Tortarolo, G.; Ahlström, A.; Doney, S.C.; Graven, H.; Heinze, C.; Huntingford, C.; et al. Recent trends and drivers of regional sources and sinks of carbon dioxide. *Biogeosciences* **2015**, *12*, 653–679. [[CrossRef](#)]
33. Wang, Q.F.; Zheng, H.; Zhu, X.J.; Yu, G.R. Primary estimation of Chinese terrestrial carbon sequestration during 2001–2010. *Sci. Bull.* **2015**, *60*, 577–590. [[CrossRef](#)]
34. Xiao, J.F.; Zhou, Y.; Zhang, L. Contributions of natural and human factors to increases in vegetation productivity in China. *Ecosphere* **2015**, *6*, 1–20. [[CrossRef](#)]
35. Li, X.R.; Zhu, Z.C.; Zeng, H.; Piao, S.L. Estimation of gross primary production in China (1982–2010) with multiple ecosystem models. *Ecol. Model.* **2016**, *324*, 33–44. [[CrossRef](#)]
36. Mo, X.G.; Liu, S.X.; Chen, X.; Hu, S. Variability, tendencies, and climate controls of terrestrial evapotranspiration and gross primary productivity in the recent decade over China. *Ecohydrology* **2018**, *11*, e1951. [[CrossRef](#)]
37. Yao, Y.T.; Li, Z.J.; Wang, T.; Chen, A.P.; Wang, X.H.; Du, M.Y.; Jia, G.S.; Li, Y.N.; Li, H.Q.; Luo, W.J.; et al. A new estimation of China’s net ecosystem productivity based on eddy covariance measurements and a model tree ensemble approach. *Agric. For. Meteorol.* **2018**, *253*, 84–93. [[CrossRef](#)]
38. Yu, P.Y.; Zhang, Y.J.; Liu, P.R.; Zhang, J.S.; Xing, W.L.; Tong, X.J.; Zhang, J.R.; Meng, P. Regulation of biophysical drivers on carbon and water fluxes over a warm-temperate plantation in northern China. *Sci. Total Environ.* **2024**, *907*, 167408. [[CrossRef](#)]
39. Wang, K.; Piao, S.; He, Y.; Liu, Y.; He, H. Spatial variations and mechanisms for the stability of terrestrial carbon sink in China. *Sci. China Earth Sci.* **2023**, *66*, 227–236. [[CrossRef](#)]
40. Bai, J.H.; Yang, F.T.; Wang, H.M.; Xu, M.J. An empirical model of gross primary productivity (GPP) and relations between GPP and its driving factors, biogenic volatile organic compounds in a subtropical coniferous plantation in China. *Atmosphere* **2023**, *14*, 1046. [[CrossRef](#)]
41. Bai, J.H.; Yang, F.T.; Xu, M.J.; Wang, H.M. Empirical models of respiration and net ecosystem productivity and their applications in a subtropical coniferous plantation in China. *Atmosphere* **2023**, *14*, 1557. [[CrossRef](#)]

42. Sitch, S.; Smith, B.; Prentice, I.C.; Arneth, A.; Bondeau, A.; Cramer, W.; Kaplan, J.; Levis, S.; Lucht, W.; Sykes, M.T.; et al. Evaluation of ecosystem dynamics, plant geography and terrestrial carbon cycling in the LPJ dynamic global vegetation model. *Glob. Chang. Biol.* **2003**, *9*, 161–185. [[CrossRef](#)]
43. Krinner, G.; Viovy, N.; de Noblet-Ducoudré, N.; Ogée, J.; Polcher, J.; Friedlingstein, P.; Ciais, P.; Sitch, S.; Prentice, I.C. A dynamic global vegetation model for studies of the coupled atmosphere-biosphere system. *Glob. Biogeochem. Cycles* **2005**, *19*, GB1015. [[CrossRef](#)]
44. O’Sullivan, M.; Friedlingstein, P.; Sitch, S.; Anthoni, P.; Arneth, A.; Arora, V.K.; Bastrikov, V.; Delire, C.; Goll, D.S.; Jain, A.; et al. Process-oriented analysis of dominant sources of uncertainty in the land carbon sink. *Nat. Commun.* **2022**, *13*, 4781. [[CrossRef](#)] [[PubMed](#)]
45. Tans, P.P.; Fung, I.Y.; Takahashi, T. Observational constraints on the global atmospheric CO₂ budget. *Science* **1990**, *247*, 1431–1438. [[CrossRef](#)] [[PubMed](#)]
46. Denning, A.S.; Randall, D.A.; Collatz, G.J.; Sellers, P.J. Simulations of terrestrial carbon metabolism and atmospheric CO₂ in a general circulation model. *Tellus B* **1996**, *48*, 543–567. [[CrossRef](#)]
47. Yao, Y.T.; Wang, X.H.; Li, Y.; Wang, T.; Shen, M.G.; Du, M.Y.; He, H.L.; Li, Y.N.; Luo, W.J.; Ma, M.G.; et al. Spatiotemporal pattern of gross primary productivity and its covariation with climate in China over the last thirty years. *Global Chang. Biol.* **2018**, *24*, 184–196. [[CrossRef](#)]
48. Wang, C.; Zhao, W.; Zhang, Y. The Change in Net Ecosystem Productivity and its Driving Mechanism in a Mountain Ecosystem of Arid Regions, Northwest China. *Remote Sens.* **2022**, *14*, 4046. [[CrossRef](#)]
49. Gupta, S.; Burman, P.K.D.; Tiwari, Y.K.; Dumk, U.C.; Kumari, N.; Srivastava, A.; Raghubanshi, A.S. Understanding carbon sequestration trends using model and satellite data under different ecosystems in India. *Sci. Total Environ.* **2023**, *897*, 166381. [[CrossRef](#)]
50. Granier, A.; Biron, P.; Lemoine, D. Water balance, transpiration and canopy conductance in two beech stands. *Agric. For. Meteorol.* **2000**, *100*, 291–308. [[CrossRef](#)]
51. Schmid, H.P.; Grimmer, C.S.; Cropley, F.; Offerle, B.; Su, H.B. Measurements of CO₂ and energy fluxes over a mixed hardwood forest in the mid-n United States. *Agric. For. Meteorol.* **2000**, *103*, 357–374. [[CrossRef](#)]
52. Baldocchi, D.D. Assessing the eddy covariance technique for evaluating carbon dioxide exchange rates of ecosystems: Past, present and future. *Glob. Chang. Biol.* **2003**, *9*, 479–492. [[CrossRef](#)]
53. Loescher, H.W.; Law, B.E.; Mahrt, L.; Hollinger, D.Y.; Campbell, J.; Wofsy, S.C. Uncertainties in, and interpretation of, carbon flux estimates using the eddy covariance technique. *J. Geophys. Res.* **2006**, *111*, D21S90. [[CrossRef](#)]
54. Friedlingstein, P.; O’Sullivan, M.; Jones, M.W.; Andrew, R.M.; Hauck, J.; Olsen, A.; Gkritzalis, T.; Gregor, L.; Gruber, N.; Harris, I.; et al. Global carbon budget 2020. *Earth Syst. Sci. Data* **2020**, *12*, 3269–3340. [[CrossRef](#)]
55. Dong, Y.X.; Yang, M.X.; Bakker, D.C.E.; Kitidis, V.; Bell, T.G. Uncertainties in eddy covariance air–sea CO₂ flux measurements and implications for gas transfer velocity parameterisations. *Atmos. Chem. Phys.* **2021**, *21*, 8089–8110. [[CrossRef](#)]
56. Nagy, L.; Bruce, R.F.; Paulo, A. (Eds.) Climate and the Amazonian Carbon Balance. In *Ecological Studies 227*; Springer Nature: Berlin/Heidelberg, Germany, 2016. [[CrossRef](#)]
57. Robinson, J.M.; O’Neill, T.A.; Ryburn, J.; Liang, L.L.; Arcus, V.L.; Schipper, L.A. Rapid laboratory measurement of the temperature dependence of soil respiration and application to changes in three diverse soils through the year. *Biogeochemistry* **2017**, *133*, 101–112. [[CrossRef](#)]
58. Remaud, M.; Chevallier, F.; Maignan, F.; Belviso, S.; Berchet, A.; Parouffe, A.; Abadie, C.; Bacour, C.; Lennartz, S.; Peylin, P. Plant gross primary production, plant respiration and carbonyl sulfide emissions over the globe inferred by atmospheric inverse modelling. *Atmos. Chem. Phys.* **2022**, *22*, 2525–2552. [[CrossRef](#)]
59. Chen, C.; Park, T.; Wang, X.; Piao, S.; Xu, B.; Chaturvedi, R.K.; Fuchs, R.; Brovkin, V.; Ciais, P.; Fensholt, R.; et al. China and India lead in greening of the world through land-use management. *Nat. Sustain.* **2019**, *2*, 122–129. [[CrossRef](#)]
60. Piao, S.; Fang, J.; Ciais, P.; Peylin, P.; Huang, Y.; Sitch, S.; Wang, T. The carbon balance of terrestrial ecosystems in China. *Nature* **2009**, *458*, 1009–1013. [[CrossRef](#)]
61. Fang, J.; Guo, Z.; Piao, S.; Chen, A. Terrestrial vegetation carbon sinks in China, 1981–2000. *Sci. China Ser. D Earth Sci.* **2007**, *50*, 1341–1350.
62. Piao, S.; He, Y.; Wang, X.; Chen, F. Estimation of China’s terrestrial ecosystem carbon sink: Methods, progress and prospects. *Sci. China Earth Sci.* **2022**, *65*, 641–651. [[CrossRef](#)]
63. Yu, G.R.; Chen, Z.; Piao, S.L.; Peng, C.H.; Ciais, P.; Wang, Q.F.; Li, X.R.; Zhu, X.J. High carbon dioxide uptake by subtropical forest ecosystems in the East Asian monsoon region. *Proc. Natl. Acad. Sci. USA* **2014**, *111*, 4910–4915. [[CrossRef](#)]
64. Zhang, Y.; Xiao, X.; Zhang, Y.; Wolf, S.; Zhou, S.; Joiner, J.; Guanter, L.; Verma, M.; Sun, Y.; Yang, X.; et al. On the Relationship between Sub-Daily Instantaneous and Daily Total Gross Primary Production: Implications for Interpreting Satellite-Based SIF Retrievals. *Remote Sens. Environ.* **2018**, *205*, 276–289. [[CrossRef](#)]
65. Wang, J.; Jiang, F.; Wang, H.; Qiu, B.; Wu, M.; He, W.; Ju, W.; Zhang, Y.; Chen, J.M.; Zhou, Y. Constraining Global Terrestrial Gross Primary Productivity in a Global Carbon Assimilation System with OCO-2 Chlorophyll Fluorescence Data. *Agric. For. Meteorol.* **2021**, *304–305*, 108424. [[CrossRef](#)]

66. Pandiyan, S.; Navaneethan, C.; Vijayan, R.; Gunasekaran, G.; Khan, K.Y.; Guo, Y. Evaluation of Drought Using Satellite Solar-Induced Chlorophyll Fluorescence during Crop Development Stage over Xinjiang, China. *Meas. J. Int. Meas. Confed.* **2022**, *187*, 110327. [[CrossRef](#)]
67. Jing, X.; Li, B.; Ye, Q.; Zou, Q.; Yan, J.; Du, K. Integrate the Canopy SIF and Its Derived Structural and Physiological Components for Wheat Stripe Rust Stress Monitoring. *Remote Sens.* **2022**, *14*, 3427. [[CrossRef](#)]
68. Qiu, R.; Han, G.; Ma, X.; Xu, H.; Shi, T.; Zhang, M. A Comparison of OCO-2 SIF, MODIS GPP, and GOSIF Data from Gross Primary Production (GPP) Estimation and Seasonal Cycles in North America. *Remote Sens.* **2020**, *12*, 258. [[CrossRef](#)]
69. Yu, G.R.; Wen, X.F.; Li, Q.K.; Zhang, L.M.; Ren, C.Y.; Liu, Y.F.; Guan, D.X. Seasonal patterns and environmental control of ecosystem respiration in subtropical and temperate forests in China. *Sci. China Ser. D* **2004**, *34*, 84–94. (In Chinese)
70. Bai, J.H.; Duhl, T. A primary generalized empirical model of BVOC emissions for some typical forests in China. *Atmos. Pollut. Res.* **2021**, *12*, 101126. [[CrossRef](#)]
71. Liu, Y.F.; Song, X.; Yu, G.R.; Sun, S.M.; Wen, X.F.; Chrn, Y.R. Seasonal dynamics of CO₂ fluxes from subtropical plantation coniferous ecosystem. *Sci. China Ser. D Earth Sci.* **2005**, *48* (Suppl. I), 123–132.
72. Xu, M.J.; Wang, H.M.; Wen, X.F.; Zhang, T.; Di, Y.B.; Wang, Y.D.; Wang, J.L.; Cheng, C.P.; Zhang, W.J. The full annual carbon balance of a subtropical coniferous plantation is highly sensitive to autumn precipitation. *Sci. Rep.* **2017**, *1*, 10025. [[CrossRef](#)]
73. Zhu, Z.L.; Sun, X.M.; Yu, G.R.; Wen, X.F.; Zhang, Y.P.; Han, S.J.; Yan, J.H.; Wang, H.M. Radiometers performance attenuation and data correction in long-term observation of total radiation and photosynthetically active radiation in typical forest ecosystems in China Chinese. *J. Appl. Ecol.* **2011**, *22*, 2954–2962.
74. Yu, G.R.; Wen, X.F.; Sun, X.M.; Tanner, B.D.; Lee, X.; Chen, J.Y. Overview of ChinaFLUX and evaluation of its eddy covariance measurement. *Agric. For. Meteorol.* **2006**, *137*, 125–137. [[CrossRef](#)]
75. Webb, E.K.; Pearman, G.I.; Leuning, R. Correction of flux measurements for density effects due to heat and water-vapor transfer. *Q. J. Roy. Meteor. Soc.* **1980**, *106*, 85–100. [[CrossRef](#)]
76. Aubinet, M.; Grelle, A.; Ibrom, A.; Rannik, Ü.; Moncrieff, J.; Foken, T.; Kowalski, A.S.; Martin, P.H.; Berbigier, P.; Bernhofer, C.; et al. Estimates of the annual net carbon and water exchange of forests: The EUROFLUX methodology. *Adv. Ecol. Res.* **2000**, *30*, 113–175.
77. Michaelis, L.; Menten, M.L. Die kinetik der invertinwirkung. *Biochem* **1913**, *49*, 333–369.
78. Lloyd, J.; Taylor, J.A. On the temperature dependence of soil respiration. *Funct. Ecol.* **1994**, *8*, 315–323. [[CrossRef](#)]
79. Falge, E.; Baldocchi, D.; Olson, R.; Anthoni, P.; Aubinet, M.; Bernhofer, C.; Burba, G.; Ceulemans, R.; Clement, R.; Dolman, H.; et al. Gap filling strategies for defensible annual sums of net ecosystem exchange. *Agric. For. Meteorol.* **2001**, *107*, 43–69. [[CrossRef](#)]
80. Reichstein, M.; Falge, E.; Baldocchi, D.; Papale, D.; Aubinet, M.; Berbigier, P.; Bernhofer, C.; Buchmann, N.; Gilmanov, T.; Granier, A.; et al. On the separation of net ecosystem exchange into assimilation and ecosystem respiration: Review and improved algorithm. *Glob. Change Biol.* **2005**, *11*, 1424–1439. [[CrossRef](#)]
81. Li, X.; Xiao, J. A Global, 0.05-Degree Product of Solar-Induced Chlorophyll Fluorescence Derived from OCO-2, MODIS, and Reanalysis Data. *Remote Sens.* **2019**, *11*, 517. [[CrossRef](#)]
82. Yang, R.; Wang, M.; Zhao, M.; Feng, X. Synergic benefits of air pollutant reduction, CO₂ emission abatement, and water saving under the goal of achieving carbon emission peak: The case of Tangshan city, China. *Int. J. Environ. Res. Public Health.* **2022**, *19*, 7145. [[CrossRef](#)]
83. Yue, X.; Unger, N. Fire air pollution reduces global terrestrial productivity. *Nat. Commun.* **2018**, *9*, 5413. [[CrossRef](#)]
84. Bai, J.H.; de Leeuw, G.; van der A, R.; Smedt, I.D.; Theys, N.; Van Roozendaal, M.; Sogacheva, L.; Chai, W.H. Variations and photochemical transformations of atmospheric constituents in North China. *Atmos. Environ.* **2018**, *189*, 213–226. [[CrossRef](#)]
85. Lee, J.D.; Drysdale, W.S.; Finch, D.P.; Wilde, S.E.; Palmer, P.I. UK surface NO₂ levels dropped by 42% during the COVID-19 lockdown: Impact on surface O₃. *Atmos. Chem. Phys.* **2020**, *20*, 15743–15759. [[CrossRef](#)]
86. Weber, J.; King, J.A.; Abraham, N.L.; Grosvenor, D.P.; Smith, C.J.; Shin, Y.M.; Lawrence, P.; Roe, S.; Beerling, D.J.; Martin, M.V. Chemistry-albedo feedbacks offset up to a third of forestation's CO₂ removal benefits. *Science* **2024**, *383*, 860–864. [[CrossRef](#)] [[PubMed](#)]
87. Bai, J.H.; Wan, X.W.; Arslan, E.; Zong, X.M. Global solar radiation and its interactions with atmospheric substances, and their effects on air temperature change in Ankara Province. *Climate* **2024**, *12*, 35. [[CrossRef](#)]
88. Liu, F.; Liu, H.Y.; Adalibieke, W.; Peng, Z.Y.; Liang, B.Y.; Feng, S.W.; Shi, L.; Zhu, X.R. Decline in stability of forest productivity in the tropics as determined by canopy water content. *iScience* **2023**, *26*, 107211. [[CrossRef](#)]
89. Niu, Y.; Li, Y.; Yun, H.; Wang, X.; Gong, X.; Duan, Y.; Liu, J. Variations in diurnal and seasonal net ecosystem carbon dioxide exchange in a semiarid sandy grassland ecosystem in China's Horqin Sandy Land. *Biogeosciences* **2020**, *17*, 6309–6326. [[CrossRef](#)]
90. Zhang, X.; Bi, J.; Zhu, D.; Meng, Z. Seasonal variation of net ecosystem carbon exchange and gross primary production over a Loess Plateau semi-arid grassland of northwest China. *Sci. Rep.* **2024**, *14*, 2916. [[CrossRef](#)]
91. Magney, T.S.; Bowling, D.R.; Logan, B.A.; Grossmann, K.; Stutz, J.; Blanken, P.D.; Burns, S.P.; Cheng, R.; Garcia, M.A.; Köhler, P.; et al. Mechanistic evidence for tracking the seasonality of photosynthesis with solar-induced fluorescence. *Proc. Natl. Acad. Sci. USA* **2019**, *116*, 11640–11645. [[CrossRef](#)]
92. Hou, X.; Zhang, B.; Chen, J.; Zhou, J.; He, Q.Q.; Yu, H. Response of Vegetation Productivity to Greening and Drought in the Loess Plateau Based on VIs and SIF. *Forests* **2024**, *15*, 339. [[CrossRef](#)]

93. Damm, A.; Elbers, J.; Erler, A.; Gioli, B.; Hamdi, K.; Hutjes, R.; Kosvancova, M.; Meroni, M.; Miglietta, F.; Moersch, A.; et al. Remote sensing of sun-induced fluorescence to improve modeling of diurnal courses of gross primary production (GPP). *Glob. Chang. Biol.* **2010**, *16*, 171–186. [[CrossRef](#)]
94. Frankenberg, C.; Fisher, J.B.; Worden, J.; Badgley, G.; Saatchi, S.S.; Lee, J.-E.; Toon, G.C.; Butz, A.; Jung, M.; Kuze, A.; et al. New global observations of the terrestrial carbon cycle from GOSAT: Patterns of plant fluorescence with gross primary productivity. *Geophys. Res. Lett.* **2011**, *38*, L17706. [[CrossRef](#)]
95. Yang, X.; Tang, J.; Mustard, J.F.; Lee, J.; Rossini, M.; Joiner, J.; Munger, J.W.; Kornfeld, A.; Richardson, A.D. Solar-induced chlorophyll fluorescence that correlates with canopy photosynthesis on diurnal and seasonal scales in a temperate deciduous forest. *Geophys. Res. Lett.* **2015**, *42*, 2977–2987. [[CrossRef](#)]
96. Yang, P.Q.; van der Tol, C. Linking canopy scattering of far-red Sun-induced chlorophyll fluorescence with reflectance. *Remote Sens. Environ.* **2018**, *209*, 456–467. [[CrossRef](#)]
97. Liu, X.; Guanter, L.; Liu, L.; Damm, A.; Malenovský, Z.; Rascher, U.; Peng, D.; Du, S.; Gastellu-Etchegorry, J.-P. Downscaling of solar-induced chlorophyll fluorescence from canopy level to photosystem level using a random forest model. *Remote Sens. Environ.* **2019**, *231*, 110772. [[CrossRef](#)]
98. Wang, Y.N.; Wei, J.; Tang, X.G.; Hang, X.J.; Ma, M.G. Progress of using the chlorophyll fluorescence to estimate terrestrial gross primary production. *Remote Sens. Technol. Appl.* **2020**, *35*, 975–989.
99. Qiu, B.; Guo, W.D. Progresses in solar-induced chlorophyll fluorescence and its applications in terrestrial ecosystem carbon cycling and land-atmosphere interaction. *Trans. Atmos. Sci.* **2022**, *45*, 801–814. [[CrossRef](#)]
100. Zhang, H.Y.; Lv, Y.J.; Li, J.K. Spatial and temporal distribution characteristics of solar energy resources and utilization in construction in Jiangxi Province. *J. Henan Univ. Urban Constr.* **2017**, *26*, 81–87. [[CrossRef](#)]
101. Liu, M.; He, H.-L.; Yu, G.-R.; Sun, X.-M.; Zhu, X.-D.; Zhang, L.; Zhao, X.-Q.; Wang, H.-M.; Shi, P.-L.; Han, S.-J. Impacts of uncertainty in data processing on estimation of CO₂ flux components. *Chin. J. Appl. Ecol.* **2010**, *21*, 2389–2396.
102. Bai, J.H. A calibration method of solar radiometers. *Atmos. Pollut. Res.* **2019**, *10*, 1365–1373. [[CrossRef](#)]
103. Wieckowski, A.; Vestin, P.; Ardö, J.; Rouspard, O.; Ndiaye, O.; Diatta, O.; Ba, S.; Agbohessou, Y.; Fensholt, R.; Verbrugge, W.; et al. Eddy covariance measurements reveal a decreased carbon sequestration strength 2010–2022 in an African semiarid savanna. *Glob. Chang. Biol.* **2024**, *30*, e17509. [[CrossRef](#)]
104. Gu, L.H.; Baldocchi, D.; Verma, S.B.; Black, T.A.; Vesala, T.; Falge, E.M.; Dowty, P.R. Advantages of diffuse radiation for terrestrial ecosystem productivity. *J. Geophys. Res.* **2002**, *107*, ACL 2-1–ACL 2-23. [[CrossRef](#)]
105. Mercado, L.M.; Bellouin, N.; Sitch, S.; Boucher, O.; Huntingford, C.; Wild, M.; Cox, P.M. Impact of changes in diffuse radiation on the global land carbon sink. *Nature* **2009**, *458*, 1014–1017. [[CrossRef](#)] [[PubMed](#)]
106. Wang, X.; Wu, J.; Chen, M.; Xu, X.; Wang, Z.; Wang, B.; Wang, C.; Piao, S.; Lin, W.; Miao, G.; et al. Field evidences for the positive effects of aerosols on tree growth. *Glob. Chang. Biol.* **2018**, *24*, 4983–4992. [[CrossRef](#)]
107. Zhou, Y.; Wu, X.; Ju, W.; Zhang, L.; Chen, Z.; He, W.; Liu, Y.; Shen, Y. Modeling the effects of global and diffuse radiation on terrestrial gross primary productivity in china based on a two-leaf light use efficiency model. *Remote Sens.* **2020**, *12*, 3355. [[CrossRef](#)]
108. Zhou, H.; Yue, X.; Lei, Y.; Zhang, T.; Tian, C.; Ma, Y.; Cao, Y. Responses of gross primary productivity to diffuse radiation at global FLUXNET sites. *Atmos. Environ.* **2021**, *244*, 117905. [[CrossRef](#)]
109. Lowe, P.R. An approximating polynomial for computation of saturation vapor pressure. *J. Appl. Meteorol.* **1977**, *16*, 100–103. [[CrossRef](#)]
110. Yu, Z.; Ciaia, P.; Piao, S.; Houghton, R.A.; Lu, C.; Tian, H.; Agathokleous, E.; Kattiel, G.R.; Sitch, S.; Goll, D.; et al. Forest expansion dominates China's land carbon sink since 1980. *Nat. Commun.* **2022**, *13*, 5374. [[CrossRef](#)]
111. Wu, D.; Shao, Q.; Li, J. Effects of afforestation on carbon storage in Boyang Lake Basin, China. *Chin. Geogr. Sci.* **2013**, *23*, 647–654. [[CrossRef](#)]
112. Li, S.P.; Matthews, J.; Sinha, A. Atmospheric hydroxyl radical production from electronically excited NO₂ and H₂O. *Science* **2008**, *319*, 1657–1660. [[CrossRef](#)]
113. Rocha, A.V.; Su, H.B.; Vogel, C.S.; Schmid, H.P.; Curtis, P.S. Photosynthetic and water use efficiency responses to diffuse radiation by an aspen-dominated northern hardwood forest. *For. Sci.* **2004**, *50*, 793–801. [[CrossRef](#)]
114. Kanniah, K.D.; Beringer, J.; Hutley, L. Exploring the link between clouds, radiation, and canopy productivity of tropical savannas. *Agr. Forest Meteorol.* **2013**, *182*, 304–313. [[CrossRef](#)]
115. Cirino, G.G.; Souza, R.A.F.; Adams, D.K.; Artaxo, P. The effect of atmospheric aerosol particles and clouds on net ecosystem exchange in the Amazon. *Atmos. Chem. Phys.* **2014**, *14*, 6523–6543. [[CrossRef](#)]
116. Bouvier-Brown, N.C.; Schade, G.W.; Misson, L.; Lee, A.; McKay, M.; Goldstein, A.H. A Contributions of biogenic volatile organic compounds to net ecosystem carbon flux in a ponderosa pine plantation. *Atmos. Environ.* **2012**, *60*, 527–533. [[CrossRef](#)]
117. Cohan, D.S.; Xu, J.; Greenwald, R.; Bergin, M.H.; Chameides, W.L. Impact of atmospheric aerosol light scattering and absorption on terrestrial net primary productivity, Global Biogeochem. Cycles **2002**, *16*, 1090. [[CrossRef](#)]
118. Knohl, A.; Baldocchi, D.D. Effects of diffuse radiation on canopy gas exchange processes in a forest ecosystem. *J. Geophys. Res.* **2008**, *113*, G02023. [[CrossRef](#)]

119. Kesselmeier, J.; Ciccioli, P.; Kuhn, U.; Stefani, P.; Biesenthal, T.; Rottenberger, S.; Wolf, A.; Vitullo, M.; Valentini, R.; Nobre, A.; et al. Volatile organic compound emissions in relation to plant carbon fixation and the terrestrial carbon budget. *Glob. Biogeochem. Cycles* **2002**, *16*, 73-1–73-9. [[CrossRef](#)]
120. Guenther, A. The contribution of reactive carbon emissions from vegetation to the carbon balance of terrestrial ecosystems. *Chemosphere* **2002**, *49*, 837–844. [[CrossRef](#)]
121. Thais, M.R.; Sitch, S.; O'Sullivan, M.; Basso, L.S.; Wilson, C.; Silva, C.; Gloor, E.; Fawcett, D.; Heinrich, V.; Souza, J.G.; et al. Synthesis of the land carbon fluxes of the Amazon region between 2010 and 2020. *Commun. Earth Environ.* **2024**, *5*, 46.
122. Chen, J.; Avise, J.; Guenther, A.; Wiedinmyer, C.; Salathe, E.; Jackson, R.B.; Lamb, B. Future land use and land cover influences on regional biogenic emissions and air quality in the United States. *Atmos. Environ.* **2009**, *43*, 5771–5780. [[CrossRef](#)]
123. Xu, L.; He, N.P.; Li, M.X.; Cai, W.X.; Yu, G.R. Spatiotemporal dynamics of carbon sinks in China's terrestrial ecosystems from 2010 to 2060. *Resources. Conserv. Recycl.* **2024**, *203*, 107457. [[CrossRef](#)]
124. Wang, J.; Feng, L.; Palmer, P.I.; Liu, Y.; Fang, S.X.; Bösch, H.; W.O'Dell, C.; Tang, X.P.; Yang, D.X.; Liu, L.X.; et al. Large Chinese land carbon sink estimated from atmospheric carbon dioxide data. *Nature* **2020**, *586*, 720–723. [[CrossRef](#)] [[PubMed](#)]
125. Bai, J.H. UV extinction in the atmosphere and its spatial variation in North China. *Atmos. Environ.* **2017**, *154*, 318–330. [[CrossRef](#)]
126. Bai, J.H.; Wan, X.W.; Chai, W.H.; Wu, Y.M.; Li, K.L.; Song, T. Study on the importance of the observational data and their accuracies. *Adv. Geosci.* **2024**, *14*, 722–732. (In Chinese) [[CrossRef](#)]

Disclaimer/Publisher's Note: The statements, opinions and data contained in all publications are solely those of the individual author(s) and contributor(s) and not of MDPI and/or the editor(s). MDPI and/or the editor(s) disclaim responsibility for any injury to people or property resulting from any ideas, methods, instructions or products referred to in the content.